American Journal of Science

THE PALEOALTIMETRY OF TIBET: AN ISOTOPIC PERSPECTIVE

JAY QUADE*, DANIEL O. BREECKER**, MATHIEU DAËRON***,
and JOHN EILER[§]

ABSTRACT. Stable isotopes provide a valuable perspective on the timing of elevation change of the Tibetan Plateau. We begin our paper by looking in depth at isotopic patterns in modern Tibet. We show that the $\delta^{18}O$ value of surface waters decreases systematically up the Himalayan front in central Nepal by about $-2.8‰/km$, in agreement with the patterns documented and modeled by previous research. On the Tibetan plateau itself there is no apparent correlation between elevation and the $\delta^{18}O$ value of flowing surface waters. Both surface waters and soil carbonates display a northward increase in $\delta^{18}O$ values, of about $1.5‰/°$ north of the Himalayan crest, even though elevation increases modestly. The isotopic increase with latitude reduces the isotope-elevation gradient for water in the northernmost plateau to -1 to $-2‰/km$.

Carbonates in both soils and lakes form at higher temperatures than assumed by previous studies on the plateau. Temperature estimates from clumped-isotope (Δ_{47}) analyses of modern soil carbonates significantly exceed mean annual air T and modeled maximum summer soil temperatures by $15.8\pm2.8°$ and 9.7 ± 2.5 °C, respectively. Similarly elevated temperatures best account for the $\delta^{18}O$ values observed in modern soil and lake carbonates.

We recalculated paleoelevations from previous studies on the plateau using both higher formation temperatures and latitude-corrected isotopic values. With one notable exception, our revised model produces paleoelevation estimates very close to previous estimates. The exception is the reconstruction from late Eocene age deposits at Xoh Xil, for which we calculate elevations that are higher and much closer to the current elevation than previously reconstructed. Therefore, there is no evidence for northward progression through time of Tibetan elevation change. Instead, the available—but admittedly very scanty—evidence suggests that much of Tibet attained its modern elevation by the mid-Eocene. A truly robust test of the various geodynamic models of uplift await expansion and replication of isotopic records all across Tibet, especially in the center and north and for >15 Ma.

Key words: Tibet, carbonates, paleoaltimetry, oxygen isotopes, uplift

INTRODUCTION

The Tibetan Plateau is the largest topographic anomaly above sea-level today, in which an area roughly the size of the western USA stands above 4500 masl (meters above sea level). Tibetan paleoaltimetry, reconstructed from a stable isotopic perspective, is the focus of this paper. Prior to India-Asia collision, the southern margin of Asia was an active magmatic arc associated with a fold- and thrust belt to the north. The elevation at which this volcano-tectonic belt stood is unknown, but whatever it was, this

* Department of Geosciences, University of Arizona, Tucson, Arizona 85721; quadej@email.arizona.edu
** Department of Earth and Planetary Sciences, University of New Mexico, Albuquerque, New Mexico 87131; breecker@jsg.utexas.edu
*** Laboratoire des Sciences du Climat et de l'Environnement, CNRS-CEA-UVSQ, F91198 Gif-sur-Yvette, France; mathieu@daeron.fr
§ Division of Geological and Planetary Sciences, California Institute of Technology, Pasadena, California 91125; eiler@gps.caltech.edu

elevated region was inherited by the Himalayan-Tibetan orogen when collision commenced in the early Tertiary (Kapp and others, 2007). The chronology of elevation change since collision is only just now coming into focus, and remains a long way from providing a robust test of the various models of uplift presented in the literature. The central aim of this paper is to examine patterns of $\delta^{18}O$ values in modern meteoric water and carbonate, to revise and summarize from an isotopic perspective the history of elevation change as it is known to date, and to suggest some directions for future work.

The use of light stable isotopes to reconstruct paleoaltitude takes advantage of the fact that the oxygen and hydrogen isotopic composition of meteoric water ($\delta^{18}O_{mw}$ and δD_{mw}, respectively) decreases with elevation, by 2 to 5‰/km globally for $\delta^{18}O$ (Poage and Chamberlain, 2001). The isotopic composition of secondary carbonates and silicates formed from these waters thereby archives paleoaltimetric information, provided (1) paleotemperature of formation can be constrained, (2) isotopic equilibrium is attained, and (3) no post-burial alteration has occurred, (4) the slope and intercept of the local isotope-elevation gradient is known or can be constrained, and (5) climate change is minimal or can be constrained. Paleoelevation can also be reconstructed from paleotemperature estimates using the clumped isotope paleothermometer (Δ_{47}) (Ghosh and others, 2006a, 2006b), in which case the temperature lapse rates must be known or assumed (it is 3-10 °C/km globally).

The use of stable oxygen and hydrogen isotope values to reconstruct paleoaltitude is a relatively new and evolving science. As with any new method, the development of stable and clumped isotopes in paleoaltitude reconstruction has been hampered by a sparse database and a simplistic view of the variables involved. We attempt to redress such limitations of previous work (including our own) by a thorough examination of oxygen isotopes in modern Tibetan water and carbonate. Our focus is on oxygen in the calcium carbonate minerals, but the calibration we present will be useful at some later date for oxygen and hydrogen in silicates or in lipids.

<div align="center">THE MODERN CLIMATE OF TIBET</div>

The climate of the Tibetan Plateau is quite varied because of its huge size, from 30 to 38 °N and 70 to 100 °E. Most rain and snow in southern Tibet fall in the summer, born by southeasterly winds of the southwest Indian Monsoon. These rains are induced by intense heating and strong convergence over Pakistan and northern India (Boos and Kuang, 2010). This produces a strong low pressure trough (the Asiatic or Pakistani heat low) that anchors the western end of the monsoonal system as it follows the northward migration of the thermal equator in the late spring. Tibet lies at the northern margins of convergence and of the accompanying rains, which are largely intercepted by the Himalaya. Across Tibet rainfall decreases westward and northward from, for example, 1300 mm/yr at Darlag in easternmost Tibet, to 436 mm/yr in Lhasa in the south-central part of the country, to 35 mm/yr at Hetian just off the northwest edge of the plateau. In southern and eastern Tibet, most (>80%) of the rainfall comes in June through September, whereas towards the west and northwest the summer rains diminish and the scant precipitation comes mainly during March-April. The source of this springtime moisture is unclear but appears to come from migratory lows originating from the interior of Asia and areas further west, possibly combined with local recycling (Tian and others, 2001, 2005). Much of Tibet receives moisture from both these sources, but it is only north-central and northwest Tibet where monsoonal rain is not dominant.

Standing at an average elevation of about 4500 m, mean annual temperature is below freezing over much of the high terrain, the major exceptions being the river valleys like the Sutlej and Tsangpo in the south where elevations fall below 4000 m. For the purposes of modeling we compiled temperature data from 15 stations in our study area, from northern India across southern Tibet. We excluded stations north of about

34°, which are much colder for a given elevation. From these data, the best fit to mean annual temperature in °C against elevation (elev) in meters above sea level (or masl) along the Himalayan front is:

$$T°C = -6.3x10^{-7} \, (elev)^2 - 2.97x10^{-3} \, (elev) + 25.18 \quad (r^2 = 0.98). \tag{1}$$

The linear fit to the temperature data of $T°C = -0.0059 \, (elev) + 26.447$ is slightly less robust at $r^2 = 0.96$. For the southern and central Tibetan plateau (28-34°N) between about $3700-6000$ m only we made use of the following relationship relating mean annual temperature in °C to elevation in masl:

$$T°C = -0.0081 \, (elev) + 35.326 \quad (r^2 = 0.83). \tag{2}$$

<center>METHODS</center>

Soil Temperature

Soil temperature was measured in June in soils from the Tingri Rongbuk area at soil depths of 48 to 56 cm. We inserted a Teflon-coated, type K Omega® thermocouple 1 to 2 cm into the wall of each pit immediately after excavating to that depth and then took a reading with a handheld digital thermometer. Lake water at Ngangla Ringsto was measured in the same way in a <10 cm of water on the lake edge in mid-June, 2010.

Water

We sampled natural water primarily from small springs and streams with small catchments, and less frequently, large rivers and freshly fallen snow. The actual elevation at which rainfall feeding these surface waters fell is obviously higher than the collection elevation. Previous workers such as Currie and others (2005) have calculated this actual or "condensation-weighted mean" elevation by considering local basin hypsometry and rainfall dependences on elevation. Because relief in our study catchments is small (~1100 m), we took a much simpler approach of taking the average of sample elevation and maximum height in catchment as the catchment correction for this effect (table 1). For small catchments such as we sampled, the potential error in this approach is likely a few hundred meters or less, much smaller than the other uncertainties in the model.

At each sample site fifteen milliliters of unfiltered water or snow was sealed with Teflon and electrician's tape into a centrifuge tube and refrigerated in the laboratory. $\delta^{18}O$ (SMOW) of water samples were measured using the CO_2 equilibration method on an automated sample preparation device attached directly to a Finnigan Delta S mass spectrometer at the University of Arizona. The δD values of water were measured using an automated chromium reduction device (H-Device) attached to the same mass spectrometer. The values were corrected based on internal lab standards, which are calibrated to SMOW and SLAP. The analytical precision for $\delta^{18}O$ and δD measurements is 0.08 permil and 0.6 permil, respectively (1σ). Water isotopic results are reported using standard δ-permil notation relative to SMOW.

Soil Carbonate

Pedogenic nodules and clast coatings were collected from freshly exposed trench faces or arroyo walls. Most local bedrock or their alluvial derivatives at our soil sites are carbonate free, making it unlikely that our samples included detrital contamination from local bedrock. Pedogenic carbonates were scraped from alluvial or bedrock clasts or sampled from nodules. Carbonate analyzed for $\delta^{18}O$ and $\delta^{13}C$ values was heated at 250 °C for 3 hours *in vacuo* before stable isotopic analysis using an automated sample preparation device (Kiel III) attached directly to a Finnigan MAT 252 mass spectrometer at the University of Arizona. Measured $\delta^{18}O$ and $\delta^{13}C$ values were corrected

TABLE 1

Isotopic composition of natural waters from Tibet

Sample #	latitude °N	°N of crest	longitude °E	elev. (m)	catchment-corrected elevation (m)	Sample type	$\delta^{18}O$ (SMOW)	δD (SMOW)	d-excess (in ‰)
TP22						Lhasa Beer	-16.2	-124	5
w1273	29.28783	1.21856	87.17605	4316	4751	lake	-7.1	-85	
w1571	32.46956	3.39238	83.18535	4444	4780	lake	-3.1	-43	
TP13	31.82570	3.79324	87.55980	4427	NA	lake	-4.9	-58	
w1371	29.50554	1.31982	86.34177	4735	5420	river	-15.7	-119	7
w1373	29.60380	1.30355	85.74180	5069	5472	river	-15.7	-124	2
w1573	32.21800	2.23677	81.24127	4592	5019	river	-13.7	-109	0
w1772	32.99252	2.67827	80.64238	4410	5195	river	-15.0	-107	13
w0281	31.13423	0.08093	79.45068	5184	5722	river	-16.9	-125	10
w0381	29.05971	1.05653	88.00035	3718	NA	river (Sutlej)	-15.0	-110	10
TP1	31.76317	3.37136	92.07803	4706	NA	snow	-13.3	-99	7
TP3	31.49860	3.27178	91.30575	4671	NA	snow	-8.4	-53	14
TP6	32.09550	4.05021	87.41302	4712	NA	snow	-7.5	-29	31
TP10	32.13428	4.13001	87.97905	4935	NA	snow	-7.2	-36	21
TP11	32.14213	4.13646	87.95282	5355	NA	snow	-7.9	-40	23
TP12	32.14665	4.14085	87.95052	5397	NA	snow	-6.3	-29	22
TP16	32.27637	4.22948	87.39595	5751	NA	snow	-1.4	13	25
TP17	32.28500	4.23777	87.39228	5997	NA	snow	-3.8	-14	16
TP18	32.28735	4.24021	87.39322	6103	NA	snow	-2.4	-2	17
TP19	32.29170	4.24403	87.38767	6216	NA	snow	-2.3	-8	10
TP20	32.29373	4.24611	87.38812	6258	NA	snow	-12.9	-93	10
TP21	32.28228	4.23499	87.39167	5897	NA	snow	-3.3	-11	16
TP24	30.68367	2.49258	91.10597	5464	NA	snow	-16.5	-90	43
TP25	30.67575	2.48440	91.10750	5535	NA	snow	-9.6	-67	10
TP4	32.07507	4.05681	89.66837	4597	4654	spring	-15.7	-130	-4
TP15	31.75592	3.72043	87.52350	4659	4851	spring	-16.8	-132	3
w1372	29.60383	1.30357	85.74175	5071	5472	spring (hot)	-18.8	-156	-5
W1271	29.05971	1.05653	88.00035	4375	4716	stream	-18.6	-135	14
W1272	29.23723	1.17153	87.20902	4493	4754	stream	-17.7	-132	10
w1374	30.14100	1.76411	85.40058	5387	5730	stream	-14.8	-109	9

TABLE 1
(*continued*)

Sample #	latitude °N	°N of crest	longitude °E	elev. (m)	catchment-corrected elevation (m)	Sample type	δ18O (SMOW)	δD (SMOW)	d-excess (in ‰)
w1471	31.06784	2.59689	85.02473	4794	5321	stream	-12.6	-96	4
w1572	32.25550	2.81964	82.34258	4463	5112	stream	-11.9	-99	-4
w1771	31.99252	1.06496	79.64239	4409	5200	stream	-16.0	-118	10
w2371	32.22481	1.25030	79.57032	4724	5187	stream	-13.2	-98	7
w2571	31.45323	0.53555	79.65760	3762	4350	stream	-17.6	-137	4
w0581	29.40036	0.88725	84.86822	4614	5120	stream	-18.6	-142	6
leier1	30.03283	1.91566	90.62777	4147	4834	stream	-17.1	-127	10
leier2	30.56315	2.31058	91.44068	4470	4988	stream	-16.0	-119	9
leier3	30.81158	2.52309	91.61853	4681	5152	steam	-15.6	-114	11
leier4	31.44490	3.42118	89.74477	4607	5029	stream	-15.3	-122	1
leier5	31.40867	3.38759	89.70848	4768	5099	stream	-14.9	-108	11
leier6	29.77692	1.49136	91.60440	3897	4689	stream	-16.6	-121	11
leier7	29.97208	1.75105	91.27447	4060	4026	stream	-15.9	-124	4
leier8	29.97018	1.83219	90.77365	4122	4303	stream	-16.5	-119	13
leier9	30.58165	2.38907	91.11460	4514	4666	stream	-16.9	-128	8
leier10	30.71158	2.52334	91.08933	4916	5082	stream	-15.7	-111	15
leier11	30.69332	2.51241	91.04587	4965	5226	stream	-15.4	-108	15
leier13	30.61175	2.46870	90.80757	4900	5323	stream	-15.2	-105	17
leier14	29.89965	1.84110	90.13905	5305	5543	stream	-18.6	-131	17
leier15	29.32553	1.31980	89.46458	3792	4629	stream	-18.1	-131	13
leier16	28.13785	0.02957	86.85432	5169	6074	stream	-19.5	-136	20
leier17	28.89468	0.84978	87.41730	5058	5387	stream	-18.2	-131	15
TP2	31.93758	3.51845	92.18945	4711	5054	stream	-14.3	-110	4
TP5	31.81948	3.78502	87.53565	4489	4927	stream	-14.7	-121	-3
TP7	32.09550	4.05021	87.41302	4712	5482	stream	-13.7	-102	8
TP8	32.07190	4.05609	87.78420	4646	5384	stream	-14.2	-111	3
TP9	32.11043	4.10975	88.05150	4788	5284	stream	-12.3	-96	2
TP23	30.07170	1.84692	91.29477	4184	4858	stream	-16.5	-126	6
w1671	31.49313	0.87691	80.13542	4406	NA	NA	-13.2	-97	8

The paleoaltimetry of Tibet: An isotopic perspective

TABLE 1
(continued)

Sample #	latitude °N	°N of crest	longitude °E	elev. (m)	catchment-corrected elevation (m)		δ¹⁸O (SMOW)	δD (SMOW)	d-excess (in ‰)
H2OJQ-2	29.96993	1.74947	91.27137	3927	4046	spring	-18.2	-141	4
H2OJQ-3	29.61960	1.42042	91.15260	3980	4134	seep	-16.7	-133	0
H2OJQ-4	29.95762	1.74633	91.22083	3940	4039	spring	-16.1	-132	-3
H2OJQ-5	30.02210	1.90557	90.62307	4104	4983	small river	-17.4	-133	6
H2OJQ-6	30.07375	1.96482	90.56683	4235	4533	spring	-17.0	-139	-3
H2OJQ-7	29.93606	1.87024	90.20820	4764	5155	seep	-18.3	-143	3
H2OJQ-8	29.92105	1.86054	90.15802	4918	5329	seep	-18.9	-141	11
H2OJQ-9	29.91895	1.86095	90.13362	5013	5635	large stream	-17.5	-128	12
H2OJQ-10	29.89317	1.83482	90.13707	5225	5544	small stream	-14.1	-103	10
H2OJQ-11	29.89211	1.83487	90.12614	5347	NA	snow	-9.9	-72	7
H2OJQ-12	29.90113	1.84473	90.11784	5204	5417	small creek	-19.2	-142	11
H2OJQ-13	29.85441	1.80062	90.09179	4861	5549	large stream	-18.5	-137	11
H2OJQ-14	29.73511	1.70105	89.87581	4566	5135	medium stream	-19.0	-147	4
H2OJQ-15	29.75885	1.72763	89.84139	4785	5244	medium stream	-19.3	-144	10
H2OJQ-16	29.75019	1.72080	89.81854	4544	4869	small stream	-19.4	-151	4
H2OJQ-17	29.72278	1.69478	89.80091	4442	4733	spring	-20.2	-157	5
H2OJQ-18	29.69141	1.66902	89.72666	4299	4628	spring	-20.2	-157	5
H2OJQ-19	29.69141	1.66902	89.72666	4299	5087	river	-18.0	-137	7
H2OJQ-20	29.69142	1.66903	89.72666	3712	NA	Tsangpo	-17.5	-135	
H2OJQ-21	29.17479	1.13778	87.50566	4085	4620	spring	-20.0	-159	1
H2OJQ-22	29.17498	1.13026	87.41925	4194	4707	medium creek	-19.7	-153	5
H2OJQ-23	29.31898	1.22945	87.00134	4367	4712	small creek	-18.8	-149	2
H2OJQ-24	29.32365	1.21996	86.88926	4516	4773	spring	-19.2	-148	5
H2OJQ-25	29.48576	1.31008	86.40173	4747	5058	spring	-20.1	-153	8
H2OJQ-26	29.40230	1.12649	85.85919	4800	5180	medium creek	-20.0	-153	7
H2OJQ-27	29.61835	0.96599	84.39135	4558	4840	small creek	-19.4	-151	4
H2OJQ-28	30.11886	1.11385	83.37097	4458	NA	pond	-13.3	-124	
H2OJQ-29	30.12295	1.09966	83.32337	4461	NA	Tsangpo	-17.7	-134	
H2OJQ-30	30.47456	1.16398	82.62367	4689	NA	Tsangpo	-16.8	-123	
H2OJQ-31	30.68568	1.08560	81.99192	4622	5304	small creek	-17.6	-133	7

TABLE 1
(*continued*)

Sample #	latitude °N	°N of crest	longitude °E	elev. (m)	catchment-corrected elevation (m)		δ¹⁸O (SMOW)	δD (SMOW)	d-excess (in ‰)
H2OJQ-32	30.68748	1.00603	81.82478	4577	5319	medium creek	-16.6	-124	9
H2OJQ-33	31.05000	0.95606	81.03333	4628	NA	large creek	-16.0	-121	7
H2OJQ-35	31.48435	1.04362	80.42628	4413	5391	small creek	-11.9	-110	-14
H2OJQ-36	31.43767	0.95185	80.35058	4679	5540	small creek	-14.3	-105	9
H2OJQ-37	31.45092	0.82527	80.12007	4524	5275	medium creek	-16.1	-117	11
H2OJQ-38	31.53415	0.81891	79.97560	4325	5194	small creek	-14.3	-106	8
H2OJQ-39	31.46889	0.63295	79.78464	3613	NA	spring	-17.9	-130	13
H2OJQ-40	31.47474	0.61211	79.74296	3523	NA	Sutlej in Zada	-14.3	-100	
H2OJQ-41	30.75320	-0.09192	79.77028	3535	NA	pond	-16.5	-123	9
H2OJQ-42	31.33770	0.50521	79.79004	3851	NA	small river	-16.4	-116	15
H2OJQ-43					NA	snow	-9.6	-67	10
H2OJQ-44	31.43562	0.89975	80.26733	4811	5573	small creek	-14.2	-103	11
H2OJQ-45	31.25098	1.09608	80.92320	4836	5265	small creek	-14.1	-97	16
H2OJQ-46	31.13879	1.01862	80.98575	4582	5414	medium creek	-16.2	-119	11
H2OJQ-47	31.17353	1.05675	80.99188	5370	NA	snow	-4.3	-16	18
H2OJQ-48	30.82038	1.22423	82.00010	4909	5444	small creek	-15.0	-111	9
H2OJQ-49	31.96849	2.98826	83.43624	4806	5241	small creek	-14.5	-109	7
H2OJQ-50	32.00894	3.11052	83.65762	4265	5440	major river	-13.0	-118	-15
H2OJQ-51	31.97645	3.11256	83.75400	4488	5068	small creek	-15.8	-125	1
H2OJQ-52	31.45763	3.39013	90.22390	4592	4980	small creek	-14.9	-117	3
H2OJQ-53	31.03710	2.88620	90.85920	4621	4964	medium creek	-12.6	-93	7
H2OJQ-54	29.61972	1.40861	91.21983	3733	4541	medium creek	-15.8	-118	9
H2OJQ-55	29.61915	1.40861	91.21672	3785	4058	tiny seep	-13.2	-114	-8
H2OJQ-56	29.63605	1.41228	91.28930	3780	4304	medium creek	-15.5	-110	14
H2OJQ-57	29.51958	1.35618	90.93888	3654	NA	Lhasa River	-16.2	-120	9
H2OJQ-58	29.32163	1.19888	90.66788	3626	NA	Tsangpo near Qixu	-17.2	-129	
H2OJQ-59	29.27543	1.18890	90.39008	3693	4653	small creek	-17.3	-132	7
H2OJQ-60	29.31745	1.27968	89.91932	3778	4675	medium creek	-18.6	-141	7
H2OJQ-61	29.29077	1.26354	89.79088	3779	4775	Rong Chu River	-16.1	-122	7
H2OJQ-62	29.27102	1.28456	88.89203	3844	NA	Nyang Chu River	-18.4	-146	2

TABLE 1
(continued)

Sample #	latitude °N	°N of crest	longitude °E	elev. (m)	catchment-corrected elevation (m)	sample type	δ^{18}O (SMOW)	δD (SMOW)	d-excess (in ‰)
H2OJQ-63	29.31797	1.33192	88.85703	3833	NA	Tsangpo at Shigatse	-16.8	-130	
H2OJQ-64	29.36988	1.37006	88.07015	3940	4125	small creek	-19.3	-148	6
H2OJQ-65	29.38437	1.38036	87.98422	3949	NA	Tsangpo	-15.9	-123	
H2OJQ-66	29.08707	1.05956	87.62160	4024	5208	large river	-17.7	-135	6
H2OJQ-67	29.20852	1.16263	87.40668	4293	NA	Lang Tso Lake	-5.5	-74	
H2OJQ-68	29.38628	1.27992	86.86882	4519	4983	medium creek	-18.7	-147	2
H2OJQ-69	29.50542	1.31314	86.30332	4772	NA	large river draing Amchok Tso	-17.1	-138	-1
H2OJQ-70	29.51950	1.02588	84.93978	4572	5779	large river	-17.9	-138	5
H2OJQ-71	29.75755	0.95723	83.93658	4587	NA	Tsangpo in narrows	-11.6	-90	
H2OJQ-73	31.19065	0.93916	80.75180	4418	NA	snow on tent	-5.3	-30	13
H2OJQ-74	31.19065	0.93916	80.75180	4418	5182	small creek draining	-16.3	-124	6
H2OJQ-75	31.46769	0.56873	79.68654	3702	NA	Guge Spring	-17.7	-133	9
H2OJQ-76	31.33430	0.57277	79.90187	3988	NA	small creek at Camp 2	-15.4	-117	6
H2OJQ-77	31.40050	0.65136	79.92153	3790	NA	Sutlej	-14.4	-104	
H2OJQ-78	29.65754	0.93411	84.16723	4569	NA	pond 180506-4	-6.3	-90	
H2OJQ-79	29.87083	1.00071	83.73647	4591	NA	pond 180506-4	-3.9	-86	
H2OJQ-80	31.16668	0.51133	80.07190	4074	5159	small river	-13.4	-94	13
H2OJQ-81	31.12047	0.49341	80.11778	4101	4903	small river	-7.3	-75	
H2OJQ-82	30.97107	0.48497	80.35010	4287	5215	river w/ glacial flour	-15.7	-112	14
H2OJQ-83	31.06805	0.70291	80.55473	4263	NA	monsoon rainstorm	-16.2	-120	
H2OJQ-84	29.52077	0.93335	84.60683	4582	NA	monsoon rainstorm	-15.5	-115	
H2OJQ-85	29.20773	1.21837	88.36905	3918	NA	Shab Chu river	-17.8	-136	6
QT1	32.43659	4.29790	86.63782	4770	5175	small stream	-13.9	-116.4	-5
QT2	32.64051	4.48460	86.52475	4770	5025	small stream	-11.0	-99.0	-11
QT3	33.06834	4.93518	86.67548	4749	6007	small stream	-12.3	-88.6	10
QT4	33.50832	5.39324	86.80372	5177	6237	small stream	-9.3	-62.0	13
QT5	33.48488	5.36309	86.75517	5440	6131	small stream	-13.2	-94.5	11
QT7	33.57347	5.47030	86.89326	4830	6237	small stream	-9.2	-65.0	9
QT8	33.59064	5.46167	86.70443	4969	6110	small stream	-9.0	-60.6	12
QT9	33.59126	5.43669	86.53333	5115	5860	small stream	-9.5	-70.4	6

Table 1
(continued)

Sample #	latitude °N	°N of crest	longitude °E	elev. (m)	catchment-corrected elevation (m)	sample type	δ18O (SMOW)	δD (SMOW)	d-excess (in ‰)
QT10	33.25483	5.11614	86.63781	4937	5780	small stream	-9.7	-82.3	-5
QT11	33.39212	5.19135	86.25446	4997	5648	small stream	-9.8	-81.8	-3
QT12	33.58658	5.35016	86.05932	5230	5266	spring	-3.3	-31.3	
QT13	33.50788	5.19585	85.68684	4974	NA	fresh snow	0.2	32.2	31
QT14	33.37067	5.05983	85.69239	5080	NA	fresh snow	1.4	51.1	40
QT15	33.23938	4.85465	85.36762	5278	5858	small stream near camp	-9.7	-62.9	15
QT16	33.25274	4.84118	85.25730	5321	6188	small stream	-8.8	-54.2	16
QT17	33.27243	4.86437	85.27151	5445	6167	same small stream	-7.2	-39.9	18
QT18	33.28445	4.87947	85.28400	5685	6167	same small stream	-4.4	-14.0	21
QT19	33.26875	4.87728	85.33960	5525	5857	small stream	-4.8	-14.2	24
QT20	33.26691	5.27668	88.33536	5657	5857	same small stream	-3.4	0.0	27
QT21	33.11752	4.66705	85.10324	4769	6118	small lake	-4.7	-56.9	
QT22	33.25728	4.82532	85.17571	5500	6007	small warm creek	-12.1	-81.8	15
QT23	33.33415	4.77547	84.70590	5310	5963	small creek, S branch	-15.5	-108.9	15
QT24	33.32651	4.76264	84.68785	5633	5930	water draining snow	-18.6	-136.0	13
QT25	33.25681		84.73368	4983	5915	stream	-2.6	-57.2	
QT26	33.35487	4.93751	85.23388	5658	6253	dribble in scree field	-11.3	-75.0	15
QT29	33.30046	4.86664	85.16835	5470	6167	small stream	-11.7	-80.4	13
11076-1	31.30662	0.33314	79.57190	4678	4775	NA		-12.6	-90
16706-3	31.19732	0.21067	79.55180	5026	5988	NA		-15.0	-112
16706-4	31.20925	0.21945	79.54698	5042	5814	NA		-11.9	-86
20706-1	31.88190	0.99820	79.71020	4341	6236	small river	-13.4	-99	7
20706-2	31.96550	1.11070	79.75517	4693	6043	stream	-13.5	-99	9
20706-3	31.99842	1.07493	79.64865	4368	6015	stream	-13.4	-102	6
20706-4	31.99842	1.07493	79.64865	4368	6027	stream	-13.2	-102	4
20706-5	32.99842	2.02543	79.57265	4368	NA	rainfall in tarp	-5.7	-55	
210706-1	32.32415	1.00567	79.05890	4960	6035	stream	-12.7	-93	8
210706-6	32.20142	1.12999	79.42338	4431	6013	from stream	-13.8	-100	11
230706-1	32.24822	1.04517	79.22745	4330	NA	rainfall on tent	-12.0	-87	
230706-2	32.99842	2.02543	79.57265	4368	6012	Stream draining the NW	-13.8	-101	9

Table 1
(continued)

Sample #	latitude °N	°N of crest	longitude °E	elev. (m)	catchment-corrected elevation (m)	sample type	δ18O (SMOW)	δD (SMOW)	d-excess (in ‰)
240706-1	31.82573	0.48891	79.03238	4863	5048	Stream draining the W	-14.3	-112	3
240706-2	31.91108	1.27641	80.10542	4534	Na	Stream draining the W	-15.2	-108	13
240706-3	31.05803	0.97086	81.04567	4752	NA	River draining the N.	-15.8	-114	12
250706-1	30.72193	0.97976	81.70267	4667	NA	pool	-14.6	-127	
250706-2	30.71540	0.97706	81.71032	4666	5820	small river	-16.9	-124	11
250706-3	30.67090	1.10204	82.05717	4757	NA	Kungyu Co. Lake		-14.8	-115
250706-4	30.64408	1.14863	82.21315	4876	5963	Inflow into Kungyu Co	-15.6	-110	14
250706-6	30.27507	1.10368	82.95203	4722	5938	River	-16.8	-123	11
250706-7	30.30405	1.12434	82.93188	4667	NA	wetland	-15.4	-116	
250706-8	30.12018	1.11645	83.37432	4599	NA	water from pond	-13.1	-125	
260706-1	29.73307	0.95053	83.98893	4577	NA	river	-15.5	-114	10
260706-2	29.71140	0.95612	84.07028	4574	5913	river	-18.9	-140	11
260706-3	29.68233	0.95330	84.15003	4571	NA	wetlands		-16.6	-140
280706-1	29.25817	1.16084	90.47745	3645	NA	rainfall	-13.6	-113	
190706-1	31.76707	0.74286	79.49468	4048	6140	river	-14.4	-107	9
Bhote Kose 1	27.6765	-0.6254	85.734267	658	770	stream	-6.8	NA	NA
Bhote Kose 2	27.8375	-0.4353	85.874033	976	1847	stream	-7.7	NA	NA
Bhote Kose 3	28.036	-0.2147	85.984983	2773	2993	stream	-9.1	NA	NA
Bhote Kose 4	28.2179	-0.0349	85.97475	3938	4861	stream	-14.3	NA	NA
2415	27.8731	-0.3966	85.889217	2415	3560	stream	-11.3	NA	NA
last resort	27.9915	-0.261	85.97605	1206	1547	stream	-9.4	NA	NA
3197	28.036	-0.2138	85.989733	3197	4114	stream	-13.7	NA	NA
3565	28.1521	-0.1006	85.97475	3565	4453	stream	-12.2	NA	NA
Arun trib 1	28.1508	0.10209	87.37665	3772	4374	stream	-9.6	NA	NA
3938 trib to BK	28.2179	-0.0362	85.968083	3938		stream	-14.3	NA	NA
Shishipangma camp	28.2568	0.01016	86.0061	4090	5108.5	stream	-14.6	NA	NA
river by Shishipangma	28.3725	0.12634	86.008533	4351	6166	stream	-18.8	NA	NA
doya la 2	28.203	0.13858	87.221433	4414	4945	stream	-16.3	NA	NA
doya la 3	28.2192	0.14923	87.169883	4612	4812.5	stream	-15.5	NA	NA
doya la 4	28.2191	0.14931	87.171433	4683	5217	stream	-16.6	NA	NA
Doya La 5	28.3524	0.21843	86.669883	4815	5662.5	stream	-18.2	NA	NA

TABLE 1
(*continued*)

Sample #	latitude °N	°N of crest	longitude °E	elev. (m)	catchment-corrected elevation (m)	sample type	δ^{18}O (SMOW)	δD (SMOW)	d-excess (in ‰)
river N of Thong La	28.5755	0.356	86.150133	4863	5230.5	stream	-19.4	NA	NA
EBC	28.1377	0.02892	86.850267	5142	6981.5	stream	-20.1	NA	NA
sping above Kharta	28.1205	0.06679	87.32525	3863	4624.5	spring	-12.4	NA	NA
Tashizong-Kharta	28.3373	0.28449	87.334717	3970	4735	spring	-19.9	NA	NA
ADD spring	28.2886	0.24265	87.405617	4016	4696	spring	-19.6	NA	NA
doya la1	28.1674	0.10857	87.274167	4118	4581.5	spring	-12.9	NA	NA
doya la 10	28.3406	0.24327	86.938617	4371	4781	spring	-20.4	NA	NA
spring south of Thon	28.3758	0.14769	86.103817	4390	4611.5	spring	-20.2	NA	NA
doya la 9	28.2587	0.16923	87.001783	4558	4724	spring	-19.2	NA	NA
doya la 8	28.252	0.16303	87.005733	4633	4783.5	spring	-18.4	NA	NA
Rongbuk-Tingri	28.3364	0.21488	86.757117	5016	5222.5	spring	-21.5	NA	NA
hermits gorge	28.1431	0.0369	86.87025	5502	6054.5	spring	-21.1	NA	NA
cp3	28.2843	0.23633	87.384167	3741	NA	soil 22cm	-13.8	NA	NA
cp3	28.2843	0.23633	87.384167	3741	NA	soil 56cm	-13.9	NA	NA
cp4	28.2867	0.20698	87.083633	4825	NA	soil 54cm	-13.5	NA	NA
cp6	28.2599	0.17026	87.000883	4564	NA	soil 48cm	-14.9	NA	NA
cp7	28.5039	0.35323	86.558317	4407	NA	soil 70cm	-15.1	NA	NA
cp8	28.5038	0.35303	86.55785	4414	NA	soil 48cm	-18.5	NA	NA
DoyaLa SW1	28.1691	0.1102	87.27425	4049	NA	soil 50cm	-14.4	NA	NA
DoyaLa SW2	28.2075	0.12865	87.091617	4967	NA	soil 50cm	-17.0	NA	NA
Tong La	28.517	0.29929	86.159717	5120	NA	soil 48cm	-16.4	NA	NA
Bhote Kose SW1	27.9262	-0.334	85.936733	1312	NA	soil 48cm	-5.7	NA	NA
Bhote Kose SW2	28.1761	-0.0763	85.976333	3754	NA	soil 55cm	-11.8	NA	NA
Ngangla Ring Tso	31.47302		83.325352	4728	NA	lake water NRC10-56-3	-3.7	-57	NA

using internal laboratory standards calibrated to NBS-19 based on internal lab standards. Precision of repeated standards is ±0.11 permil for $\delta^{18}O$ (1σ). Carbonate isotopic results are reported using standard δ-permil notation relative to VPDB.

Clasts set aside for clumped-isotope analysis were rinsed with de-ionized water and dried using compressed air. Carbonate coatings were scraped off the clasts using a stainless steel dental pick, then ground and homogenized in an agate mortar. This carbonate was not heated prior to analysis, unlike carbonate used for $\delta^{18}O$ and $\delta^{13}C$ determinations. Clumped-isotope compositions of these carbonate powders were analyzed at the California Institute of Technology using protocols described by Ghosh and others (2006b), Affek and others (2008) and Huntington and others (2009). 7 to 10 mg aliquots were digested overnight at 25 °C in anhydrous orthophosphoric acid. After cryogenic trapping, the resulting CO_2 was purified of potential isobaric contaminants by passage through a dry ice/ethanol slush and a 30-m-long 530 μm ID Supelco GC column held at −10 °C. CO_2 was then analyzed using a Finnigan MAT 253 dual-inlet mass spectrometer configured for isotope ratio measurements of masses 44 to 49. Bulk composition ($\delta^{13}C$ and $\delta^{18}O$) was computed from these measurements using a reference CO_2 tank of known isotopic composition, and Δ_{47} was derived from comparison with stochastic gases, that is CO_2 in a thermodynamic state of randomly distributed isotopes, with $\Delta_{47} = 0$, obtained by heating CO_2 aliquots at 1000 °C.

CALIBRATING THE TIBETAN PALEOALTIMETER: RESULTS AND DISCUSSION

Most of our samples come from the southern half of Tibet south of about 34 °N, west of Lhasa (92 °E) and east of Zhada (78 °E) (fig. 1). We also report on samples from an elevation transect in central Nepal along Bhotse Khola.

$\delta^{18}O$ and δD Patterns from Meteoric Water

We measured a total of 245 $\delta^{18}O$ and δD values of meteoric waters (denoted $\delta^{18}O_{mw}$ and δD_{mw}, respectively) for this project, most of them from small streams and springs, but also from large rivers such as the Tsangpo, Sutlej, and Arun, as well as May to June snows, and a few ponds and lakes (table 1). Most of the water was sampled in late spring or summer of 2004 and 2006. Tibet water sampling sites were obtained from a wide range of elevations from 3600 to 6000 m, and sampling elevations show a slight tendency to increase northwards, reflecting the gradual gain in mean minimum elevations northward onto the Qiangtang Terrane of central Tibet (figs. 1 and 2).

Most of the natural waters fall along the Global Meteoric Water Line (fig. 3A), suggesting that most waters undergo little to no evaporation prior to sampling, despite the relatively arid climate, especially of western Tibet. Exceptions to this are a few of the streams, and most of the ponds and lakes, which lie to the right of the Global Meteoric Water Line. Interestingly, most of the May to June snow samples had higher $\delta^{18}O_{mw}$ and δD_{mw} values than the surface waters sampled at the same time of year.

Deuterium excess (d) is defined as: $d = \delta D_{mw} - 8\delta^{18}O_{mw}$, which we calculated for all 206 unevaporated waters in our sample set (table 1; fig. 3B). The excess for the Global Meteoric Water Line is ~ +10. In general we found that May-June snow samples display higher d values (+8 to +45) than surface waters (−15 to +20) sampled at the same time of year.

Spatial Patterns

In Nepal we measured $\delta^{18}O_{mw}$ only for small streams, springs, and soil water along an elevation transect paralleling Bhotse Khola from 658 masl elevation to the Himalayan crest near Rongbuk. $\delta^{18}O_{mw}$ decreases very regularly northward and with elevation gain (fig. 4) from 658 masl at the lowest sampling location to 5502 masl at the highest. The correlation with elevation is:

$$\delta^{18}O_{mw}(SMOW) = -1.0x10^{-7}(elev_{catch})^2 - 0.0015(elev_{catch}) - 6 \quad (r^2 = 0.63) \qquad (3)$$

where $\delta^{18}O_{mw}$ (SMOW) values are from stream and spring water and $elev_{catch}$ is the catchment-corrected elevation in masl. The y intercept has been forced through -6 permil, the isotopic composition New Delhi rainfall, consistent with previous studies (Garzione and others, 2000a; Rowley and Garzione, 2007). The $\delta^{18}O$ values of soil water are in better agreement with stream water $\delta^{18}O$ values if the elevations assigned to stream samples are catchment corrected (fig. 4).

Further north in Tibet, there is a clear relationship between $\delta^{18}O_{mw}$ and latitude ($r^2 = 0.66$) (fig. 5A) but not longitude ($r^2 = 0.05$). To examine this in another way we plotted $\delta^{18}O_{mw}$ against degrees of latitude north (°N) of the Himalayan crest (fig. 5B), which varies with latitude and can be described by:

$$\delta^{18}O_{mw}(SMOW) = 1.48x°N - 18.3. \qquad (4)$$

This relationship ($r^2=0.44$) is less robust than for the simple latitude/$\delta^{18}O_{mw}$ relationship ($r^2 = 0.66$), but we will adopt it for paleoelevation reconstruction later in the paper because distance north of the Himalayan crest for a given site changed much less than paleolatitude through time. In Tibet, there is no apparent relationship ($r^2 = 0.009$) of $\delta^{18}O_{mw}$ values with catchment-corrected elevation (fig. 6) detrended for latitude.
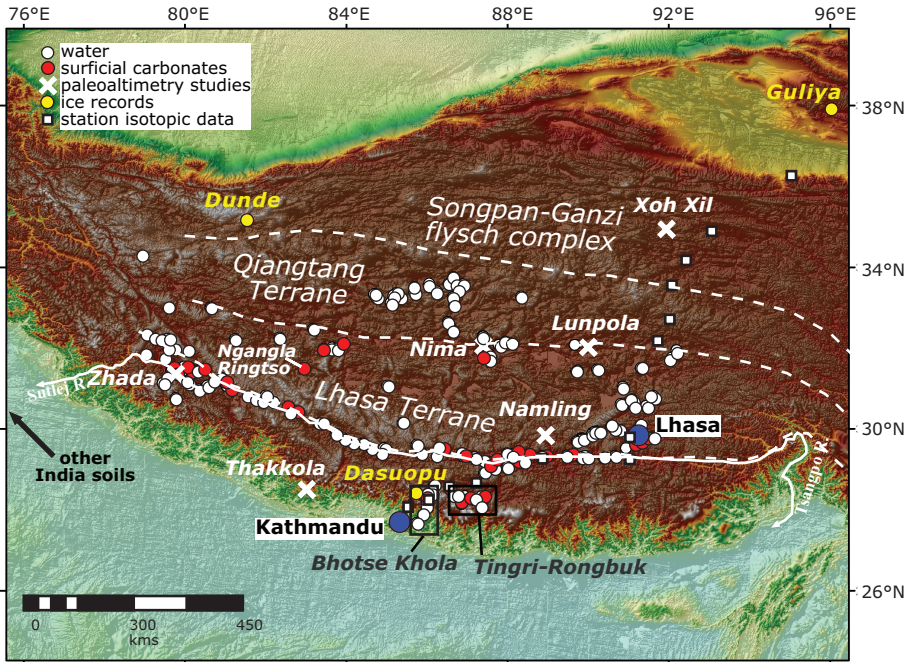
Fig. 1. Digital elevation model of the Himalaya-Tibet orogen overlaid with water (white) and soil (red) sample locations. Ice studies (yellow dots) are by Thompson and others (2003), and station data (white squares) from Tian and others (2001). Location of oxygen isotope paleoaltitude studies shown by white "x"s. Major cities shown by blue circles. The major geologic terranes discussed in the text are labeled and their boundaries indicated by dashed lines. Soils studied in NW India are off the map; locations can be found in table 2.

Discussion

Our comprehensive analysis of modern natural waters in southern Tibet, although only a two-year snapshot, reveals several patterns (fig. 7) relevant to understanding modern climate and to reconstructing paleoaltimetry. Nearly all flowing natural waters fall along or near the Global Meteoric Water Line, indicating that waters, even in arid Tibet, undergo negligible evaporation prior to recharge. Standing water plots well to the right of the Global Meteoric Water Line, mostly in a rather narrow range of -7 to -3 permil, a reflection perhaps of a narrow range of cold temperatures and low relative humidity across the plateau as standing water evaporates.

Our oxygen isotope results from flowing water, springs, and soil waters from a transect along Bhotse Khola and the Tingri-Ronbuk area show a clear correlation with elevation (fig. 4). The transect waters change by about -2.8‰/km, consistent with gradients estimated by Garzione and others (2000a) along the Kali Gandaki and modeled by Rowley and others (2001) (fig. 4).

In our sample, snowfall tends to display higher $\delta^{18}O$ and δD values (fig. 3A), and higher deuterium excesses ($> +10$; fig. 3B) than natural waters from the same area. This distinction arises from the seasonal differences of moisture sources in the region, as visible from the rainfall time series from Lhasa (IAEA). Summer rainfall there is summer monsoonal. In the winter half year the westerlies dominate, and moisture likely derives from western sources like the Mediterranean and the interior of Asia, perhaps combined with local re-evaporation off of the many lakes in Tibet. The summer versus winter contrast in $\delta^{18}O$ and δD values and higher deuterium excesses in
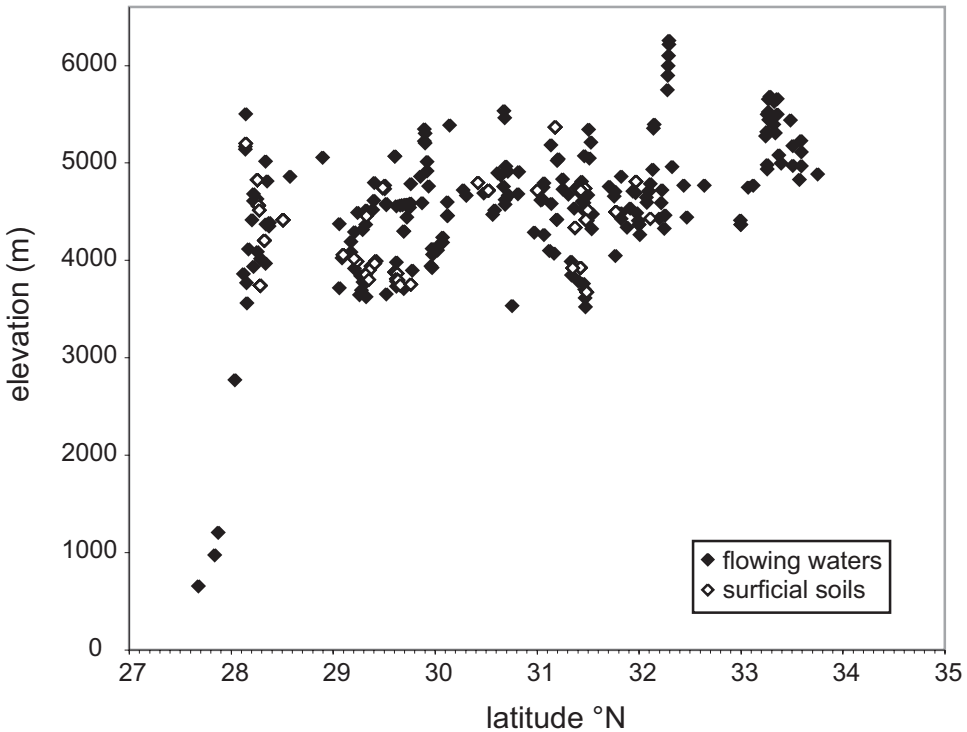
Fig. 2. Latitude of samples versus sampling elevation for flowing waters and surficial soils. Once on the plateau at ~28.5 °N, minimum sampling elevation tends to modestly increase northwards.
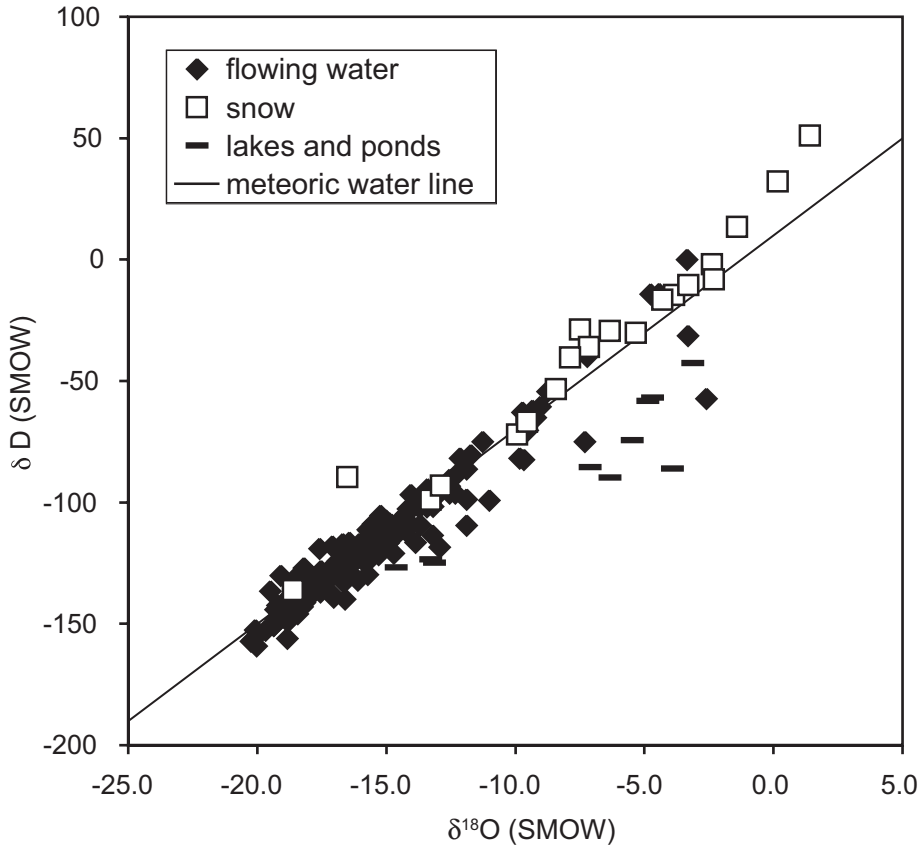
Fig. 3(A). δ^{18}O (SMOW) versus δD (SMOW) plot of all water and snow samples from Tibet obtained in this study in comparison to the global meteoric water line.

winter precipitation from Lhasa (Tian and others, 2001) are consistent with our flowing water/snow comparison. The high deuterium excesses of springtime rainfall are consistent with low-humidity source areas in the interior, and the lower excesses with humid monsoonal sources to the south.

As most of our stream samples were taken in the non-monsoon season (late spring), this means that we were sampling stream base-flow probably recharged from the previous monsoon season. We interpret this to indicate that the summer monsoon dominates the flux passing through the surficial reservoirs in southern Tibet, including our main geologic archives, such as soils and lakes.

In a huge and topographically varied area like Tibet and the Himalayas, some other influences to consider on the isotopic composition of rainfall include latitude, longitude, and elevation. As previously noted, δ^{18}O$_{mw}$ values from our transect along Bhotse Khola show a strong correlation with elevation close to that for data sets from the Kali Gandaki and Seti in west-central Nepal (Garzione and others, 2000a), the Brahmaputra (Tsangpo) system in eastern India (Hren and others, 2009), and as modeled by Rowley and others (2001). Once on the plateau the clearest correlation is with latitude: the δ^{18}O value of water decreases by about 1.5‰/°N of the Himalayan crest (fig. 5B), from average δ^{18}O (SMOW) values of about −20 permil along the
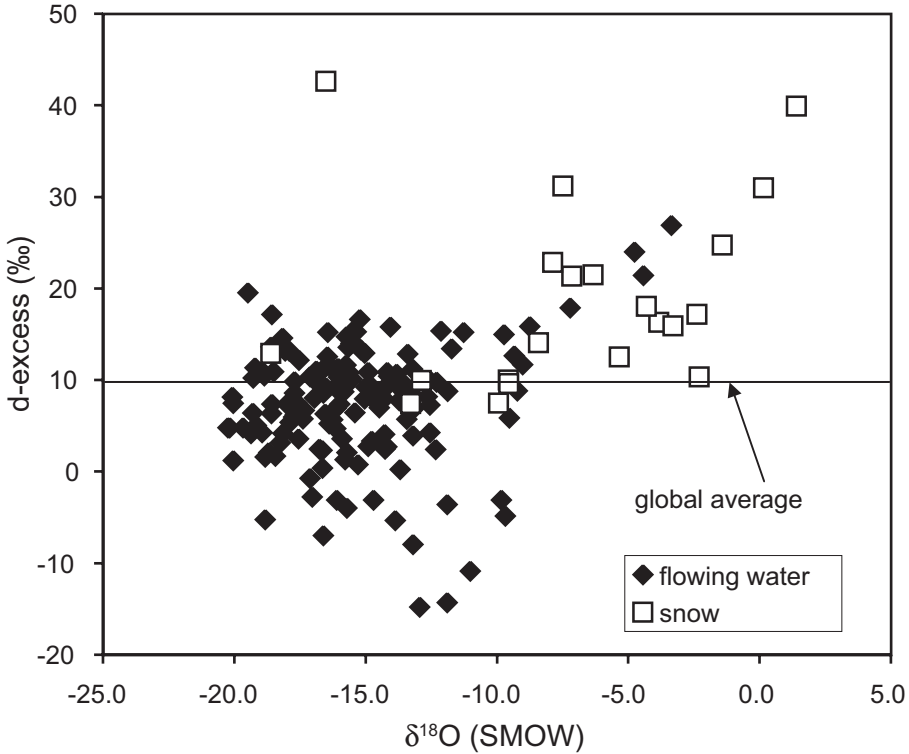
Fig. 3(B). $\delta^{18}O$ (SMOW) versus d-excess (in ‰; see text) for flowing waters and late spring snow in Tibet. The line for d = +10 (the excess displayed by the canonical global meteoric water line) also shown.

Himalayan crest to −13 permil in the mid-plateau at around 33°N (fig. 7B). There is no clear correlation with longitude.

The strong latitudinal pattern in isotopic values is visible in other data sets from streams (Hren and others, 2009) and rainfall (Tian and others, 2001). Tian and others (2001) report on analysis of monthly rainfall from a series of seventeen stations (fig. 1) from southern Tibet that show a clear progression (fig. 7B) from low (south) to higher (north) $\delta^{18}O$ values, as well as increasing deuterium excesses northward. Monthly rainfall follows $\delta^{18}O = 1.64 \times (°\text{North of crest}) - 19.645$ ($r^2 = 0.93$). Thompson and others (2003) document a similar north-south isotopic pattern on high elevation ice (fig. 7B). Thousand year averages of $\delta^{18}O$ values from Dasuopu (N°28; 7200 m; −20.3‰), Dunde (N°35; 5325 m; −14.2‰), and Guliya (N°38; 6710 m; −10.82‰) ice define the line $\delta^{18}O = 1.17 \times (°\text{N of crest}) - 20.464$ ($r^2 = 0.99$). The slopes of the station data (1.64) and long-term ice data (1.17) bracket the slope of the best linear fit to our stream data set (1.48). The y-intercept for the long-term ice averages is more negative by about 2 permil than that for modern streams and rainfall, suggesting a recent increase in isotopic composition of rainfall (Thompson and others, 2003).

The northward increase in $\delta^{18}O_{mw}$ likely reflects the diminishing contribution of ^{18}O-depleted summer monsoon rainfall in favor of springtime precipitation derived from a marine and or interior continental source to the west (Tian and others, 2001; Zhang and others, 2002; Hren and others, 2009). The northward increase in $\delta^{18}O_{mw}$ is especially interesting because elevation increases modestly from south to north in Tibet. This translates into a decrease in the isotope-elevation gradient from −2.8‰/km
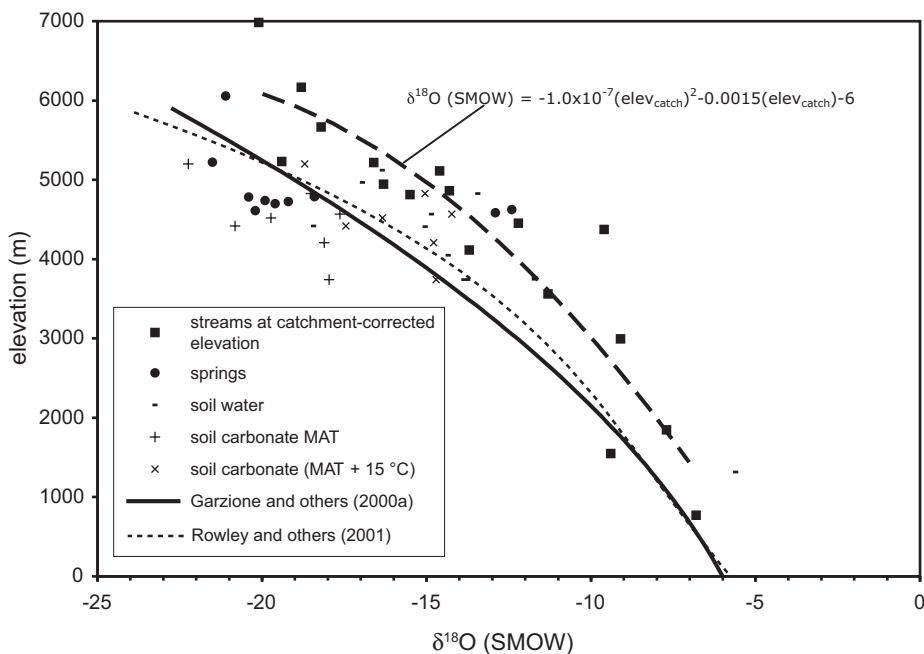
Fig. 4. Transect data along Bhotse Khola and the Tingri-Rongbuk areas (see fig. 1 for location). Observed $\delta^{18}O$ (SMOW) values of spring, stream, and soil water are compared to the stream water data set of Garzione and others (2000a) from the Kali Gandaki in Nepal, and numerical model output of Rowley and others (2001). The correlation between the catchment-corrected elevations and $\delta^{18}O$ (SMOW) values of water shown here (coarse dashed line) is equation 3 in text. Note that the axes in the equation are switched compared to the graph for ease of computation. $\delta^{18}O$ (SMOW) values of water in oxygen isotope equilibrium with measured $\delta^{18}O$ values of Holocene-age soil carbonate from the Tingri-Rongbuk area are also shown. Mean annual temperature (MAT) and MAT+15 °C were used to calculate $\delta^{18}O_{mw}$ values from $\delta^{18}O$ values of soil carbonate.

in southern Tibet to -1 to -2‰/km in northern Tibet at latitude 35 to 37 °N. The modest isotope-elevation gradient for northeastern Tibet at 34 to 35 °N has been documented by Garzione and others (2004), although in detail the gradient does not appear to be linear. The large difference in isotope-elevation gradients in southern and northern Tibet has major implications for paleoaltimetric reconstruction of Tibet, and shows that a single isotope-elevation gradient is not appropriate for the entire plateau, as already stressed in Quade and others (2007) and Hren and others (2009).

The decreases in $\delta^{18}O_{mw}$ values visible in our results both southwards and northwards of the Himalayan crest are typical for low-latitude mountain ranges, as pointed out in Blisniuk and Stern (2005). In some cases, mixing of distinct moisture sources, as in the case of Tibet, is the cause. In others, intense cloud-base evaporation produces "pseudo-altitude" changes in $\delta^{18}O_{mw}$ on the lee side of mountain ranges. Whatever the cause, the lapse rates on opposite sides of such mountain ranges are often asymmetric (Blisniuk and Stern, 2005).

It is significant that our $\delta^{18}O_{mw}$ and δD_{mw} values do not appear to correlate with elevation within the plateau itself (fig. 6), since the correlation is so strong for the Nepal elevation transects. Likewise, no elevation effect is visible in $\delta^{18}O$ values from the weather station data of Tian and others (2001) compared to that from recent ice (fig. 7) despite 3000 to 3500 meters of elevation difference. Results described in Tian and others (2007) suggest this is related to an increase in the proportion of winter-westerly
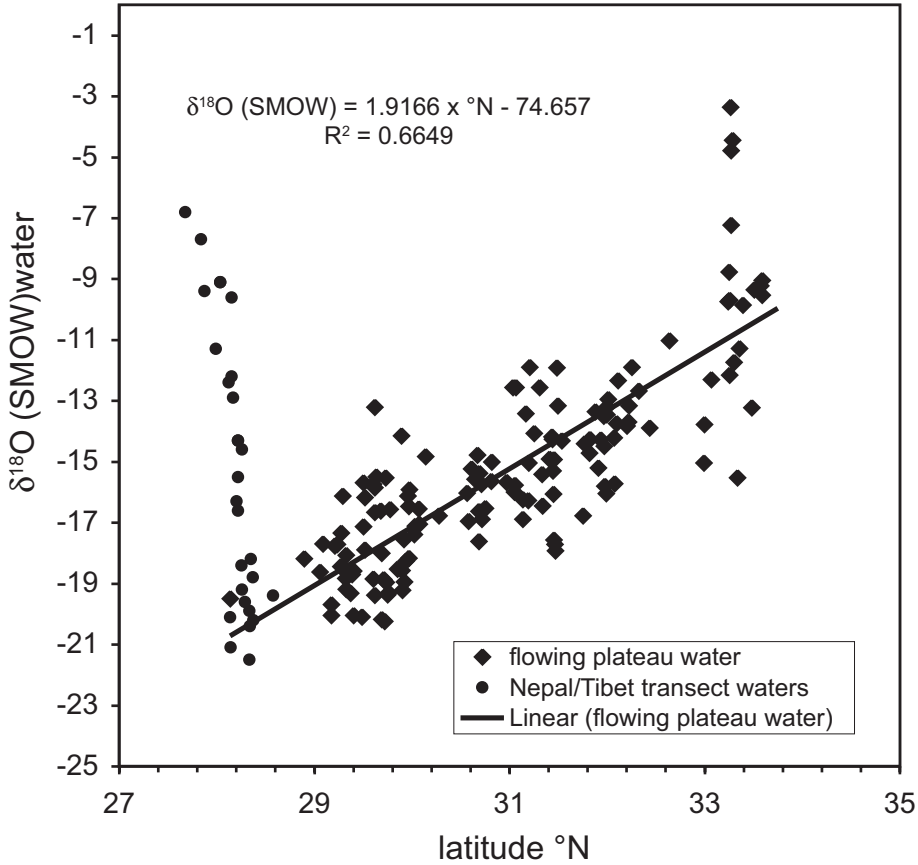
Fig. 5(A). $\delta^{18}O$ (SMOW) of unevaporated flowing waters in Tibet and Nepal versus °N latitude. The linear best fit of this relationship is shown.

compared to monsoonal moisture with elevation gain in southern Tibet. They observe much higher deuterium excesses in snow and ice from higher elevations in southern Tibet such as Dasuopu, and in amount-weighted precipitation from Nyalam in the Himalaya. The mixing with high $\delta^{18}O_{mw}$ values from winter-westerly moisture would reduce or even reverse the rather uniform elevation-isotope gradient of $-2.6°/km$ south of the Himalayan crest produced by dominantly monsoonal rainfall. The key point is that so far we cannot distinguish 4000 from 5500 masl on the Tibetan plateau using modern water data.

Soil Carbonate

We sampled calcium carbonate from more than 40 surficial (Quaternary-age) soil profiles from across northern Nepal and southern Tibet and obtained ~240 individual oxygen ($\delta^{18}O_{cc}$ values) and carbon isotope analyses (table 2), although we only discuss $\delta^{18}O_{cc}$ values here. Our treatment of these results falls in four parts, in which we look at ages of the carbonate, and soil temperature estimates based on Δ_{47} analyses from four soils. We then turn to some detailed profile measurements of soil water, local soil temperature, and carbonates along the Bhotse Khola transect in Nepal north of Kathmandu and the Tingri-Rongbuk area of Tibet, and follow this with an examination of regional patterns of $\delta^{18}O_{cc}$ values across southern Tibet.
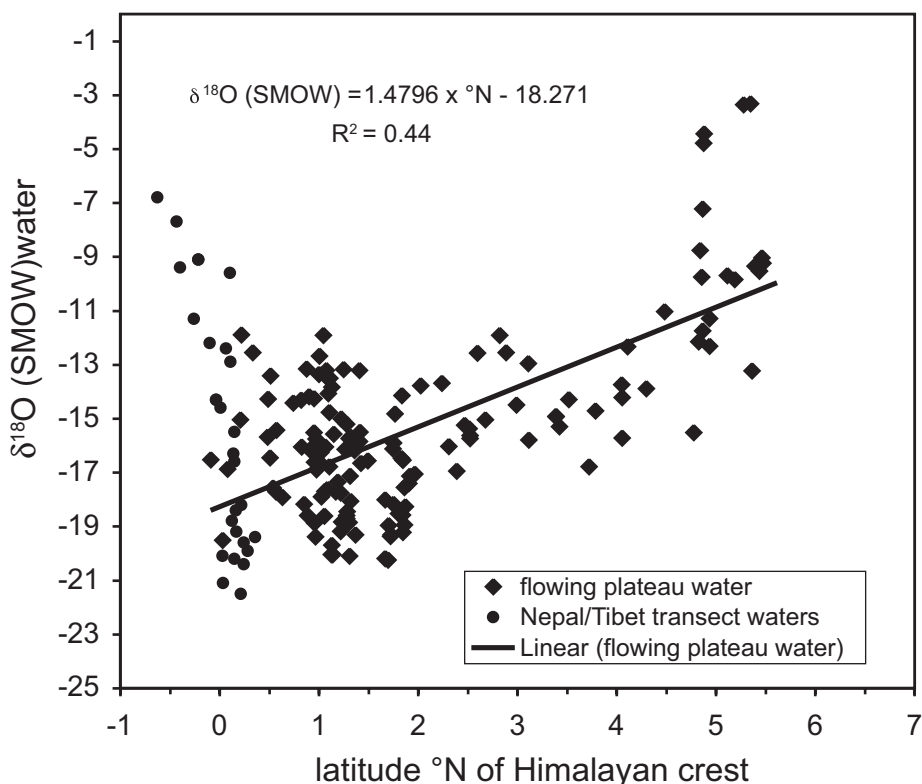
Fig. 5(B). δ^{18}O (SMOW) of unevaporated flowing waters in Tibet and Nepal with reference to the Himalayan crest, defined as 0°N. The linear best fit of this relationship is shown.

Age of soils.—Surface soils across Tibet display a range of ages which, in the absence of radiometric dating, can be semi-quantitatively evaluated based on soil morphology. As in our previous work, we use the scheme developed by Gile and others (1966) in which development of a calcareous horizon is assigned stages I–IV, Stage I being the youngest and least mature, and Stage IV the oldest (table 2). In our regional study of Tibetan soil carbonate we deliberately sampled from a range of stages on the expectation that they would record some mix of current and past conditions during the Quaternary. Monsoonal rainfall is thought to have varied on a precessional time scale with a ~23 ka periodicity. And thus, very weakly developed soils (Stage I; table 2) should be dominated by carbonate formed in the last few thousand years when the monsoon has been relatively weak. By contrast, more mature soils (Stage II+; table 2) should contain carbonate formed ($>10^4$ yrs) under both strong and weak monsoon conditions.

At Bhotse Khola and around Rongbuk we sampled more selectively than in the regional sampling, focusing only on the youngest soils and terraces so that modern water and carbonate δ^{18}O values could be directly compared. The river terraces from which pedogenic carbonate samples were collected are probably late Holocene in age. The terraces were not dated in this study, but the lowest river terraces along the Kali Gandaki River in the central Himalayas are younger than 2000 years (Hurtado Jr. and others, 2001). Holocene terrace formation in the Himalayas has been interpreted to result from regional climate variations in at least two studies (Hurtado Jr. and others,
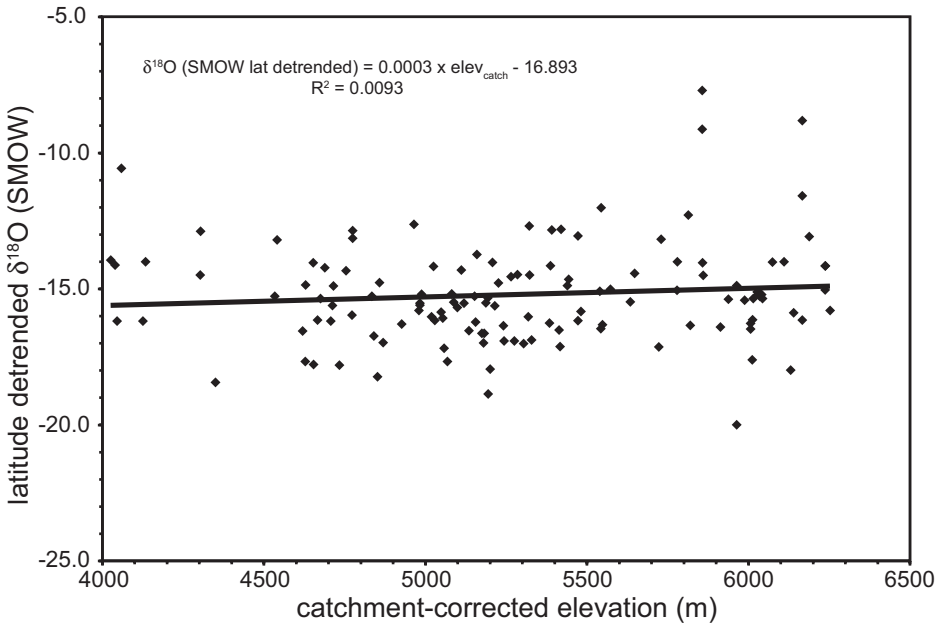
Fig. 6. Latitude-detrended $\delta^{18}O$ (SMOW) value of unevaporated flowing waters on the Tibetan Plateau versus average catchment elevation (see text).

2001; Bookhagen and others, 2006). Therefore incision and terrace formation probably occurred synchronously in most drainages in the Himalayas. The weak soil development and proximity to modern river level for the terraces studied here support the interpretation of late Holocene ages. Therefore the pedogenic carbonate in the soils sampled probably records the $\delta^{18}O$ value of meteoric water over the past several hundred to thousands of years.

   "Clumped isotope" (Δ_{47})-based temperatures from modern soils.—We obtained nine Δ_{47} analyses of carbonates from four different surficial soil profiles (table 3). The carbonates come from mature soils displaying Stage II–III carbonate development (table 3), and hence probably required 10^4 to 10^5 years to form. One analysis (table 3: TSP-21Bc) was rejected due to high (>2.0) Δ_{48}. The highest elevation soil at 4800 masl yielded the lowest Δ_{47} temperatures, whereas the three soils from the 3800 to 4000 masl range returned Δ_{47} temperatures of 17.2 to 23.5 °C. These temperatures exceed estimated local mean annual temperature by 15.8±2.8 °C using equation 2.

   The current soil depth of these samples is 50 to 110 cm, where seasonal extremes in air temperatures will be attenuated. We modeled these depth attenuation effects on temperature following the general approach described in Quade and others (2007), and compared these modeled soil temperatures to Δ_{47}-based temperatures (fig. 8). We found Δ_{47}-based temperatures exceed maximum monthly temperatures adjusted for the depth attenuation effect by 9.7±2.5 °C.

   The large departures between Δ_{47}-based temperatures and modeled temperatures must arise from (1) lack of attainment of isotopic equilibrium prior to carbonate formation, (2) non-Holocene soil temperatures, or (3) inappropriate modeling of soil temperature due to extreme summer heating of the bare soils on the plateau (for example Bartlett and others, 2006). We provisionally favor explanation (3). Adoption of pre-Holocene (glacial) temperatures would only accentuate the discrepancies that
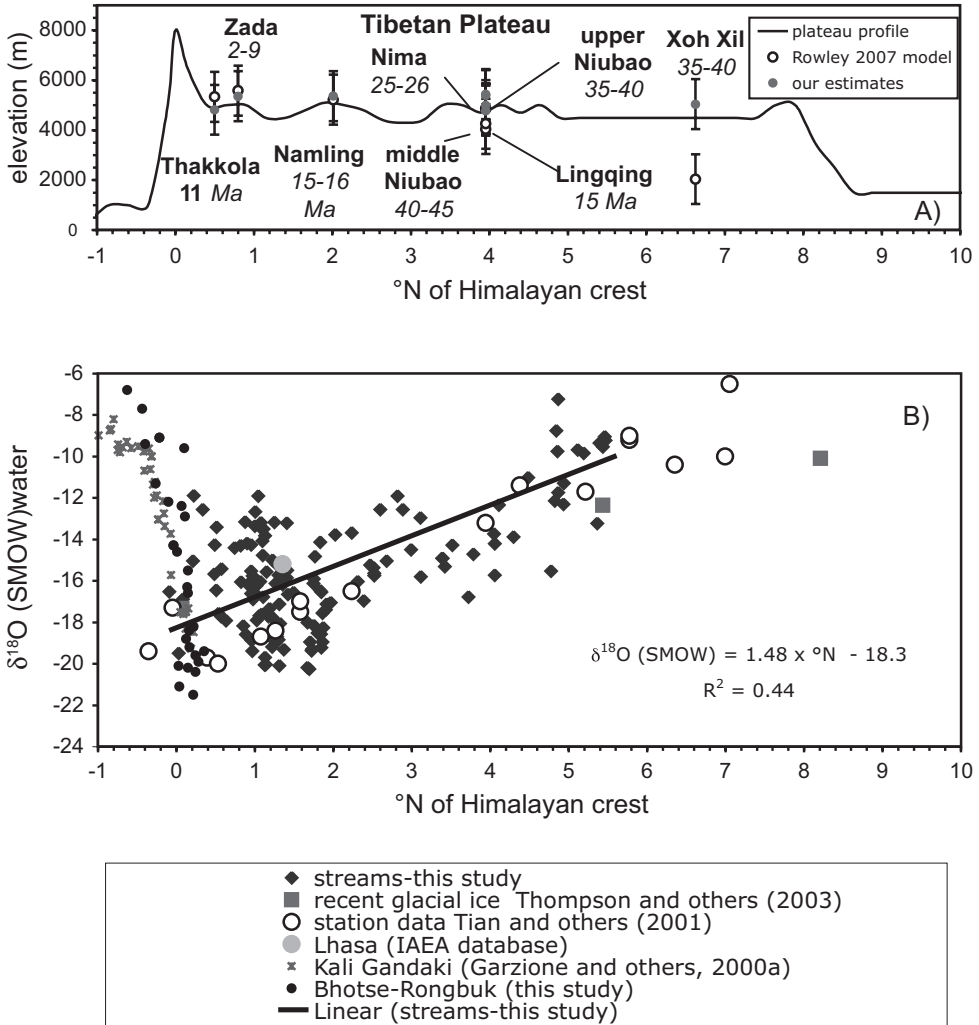
Fig. 7. (A) Generalized elevation profile across the Himalaya and Tibetan Plateau as reference for site locations in lower panel, and reconstructed paleoelevations for the studies and time periods indicated. Open circles are paleoelevations using data from previous studies and the Rowley and Garzione (2007) model. Solid circles are paleoelevations estimated in this study. (B) Summary diagram of the $\delta^{18}O$ (SMOW) value of water and ice across Nepal and Tibet. The best-fit equation for flowing surface water samples collected on the Tibetan Plateau from this study is also shown.

we observe. Non-equilibrium effects seem unlikely given the attainment of synthetic, non-biological calcites under laboratory conditions (Ghosh and others, 2006a), and the slow process of calcite formation in soils from gradual dewatering over weeks and months in the summertime (Breecker and others, 2009). This slow process ensures attainment of isotopic equilibrium between phases for ^{13}C, ^{12}C, and ^{18}O, ^{17}O, ^{16}O species (Cerling and Quade, 1993). The discrepancy between modeled and Δ_{47}-based temperatures can only be resolved by actual measurements of soil temperature over at least a year. Short of that, in the next section we examine the performance of Δ_{47}-based temperatures in predicting $\delta^{18}O_{cc}$ values from local $\delta^{18}O_{mw}$ values.

TABLE 2

Stable isotopic results from surficial carbonates in Tibet and India

sample #	$\delta^{13}C$ (PDB)	$\delta^{18}O$ (PDB)	Depth (cm)	elevation (m)	°N	°E	description*
Lhasa area							
JUP-1 60-70A	-0.77	-17.73	65	3878	29.60353	91.15838	Stage I
JUP-1 60-70B	-0.90	-16.37	65	3878	29.60353	91.15838	Stage I
JUP-1 60-70C	-0.50	-18.62	65	3878	29.60353	91.15838	Stage I
JUP-1 0-10A	-0.24	-15.16	5	3878	29.60353	91.15838	Stage I
JUP-1 0-10B	-0.16	-13.76	5	3878	29.60353	91.15838	Stage I
JUP-1 0-10C	1.83	-12.01	5	3878	29.60353	91.15838	Stage I
JUP-1 1.1A	3.85	-14.91	110	3878	29.60353	91.15838	Stage I
JUP-1 1.1B	5.41	-12.12	110	3878	29.60353	91.15838	Stage I
JUP-1 1.1C	5.22	-12.49	110	3878	29.60353	91.15838	Stage I
JUP-2 30-40B	-5.17	-11.22	35	3878	29.60353	91.15838	Stage I
JUP-2 30-40C	-5.29	-11.76	35	3878	29.60353	91.15838	Stage I
JUP-2 (0.6)A	-4.14	-14.06	60	3878	29.60353	91.15838	Stage I
JUP-2 (0.6)B	-4.63	-13.68	60	3878	29.60353	91.15838	Stage I
JUP-2 (0.6)C	-4.37	-11.99	60	3878	29.60353	91.15838	Stage I
JUP-2 (0.6)D	-4.21	-10.68	60	3878	29.60353	91.15838	Stage I
JUP-3 1.2A	-0.54	-13.74	120	3878	29.60353	91.15838	Stage III
JUP-3 1.2B	0.10	-13.62	120	3878	29.60353	91.15838	Stage III
JUP-3 1	-0.42	-14.44	120	3878	29.60353	91.15838	Stage III
JUP-4 A	-1.66	-11.61	100	3867	29.62795	91.15150	Stage I
JUP-4 B	-1.14	-12.60	100	3867	29.62795	91.15150	Stage I
JUP-4 C	-2.15	-15.27	100	3867	29.62795	91.15150	Stage I
JUP-4 D	1.49	-15.69	100	3867	29.62795	91.15150	Stage I
LHS-3A	-3.10	-14.48	30	3809	29.61980	91.21758	Stage III
LHS-3B	-2.72	-13.89	100	3809	29.61980	91.21758	Stage III
LHS-3C	-2.97	-14.72	150	3809	29.61980	91.21758	Stage III
LHS-4A	-2.48	-13.51	60	3800	29.63620	91.29172	Stage II/III
LHS-4B	-4.89	-15.56	60	3800	29.63620	91.29172	Stage II/III
LHS-4C	-3.98	-17.24	60	3800	29.63620	91.29172	Stage II/III
LHS-5A	-2.13	-12.81	75	3745	29.65715	91.32085	Stage II/III
LHS-5B	-0.26	-10.86	75	3745	29.65715	91.32085	Stage II/III
LHS-5C	0.05	-9.53	75	3745	29.65715	91.32085	Stage II/III
LHS-7A	-0.23	-16.57	50	3754	29.75938	91.50308	Stage I
LHS-7B	-0.27	-17.07	50	3754	29.75938	91.50308	Stage I
LHS-8A	-2.77	-22.46	60	3754	29.75938	91.45790	Stage I
LHS-8B	-1.29	-17.80	60	3754	29.75938	91.45790	Stage I
Tsangpo transect							
TSANGPO1 61-7OA	1.77	-16.03	65	3993	29.41975	88.25762	Stage I
TSANGPO1 61-70B	2.53	-14.11	65	3993	29.41975	88.25762	Stage I
TSANGPO1 61-70C	3.13	-15.61	65	3993	29.41975	88.25762	Stage I
TSANGPO1 61-70D	2.51	-15.71	65	3993	29.41975	88.25762	Stage I
TSANGPO1 61-70E	2.22	-15.60	65	3993	29.41975	88.25762	Stage I
TSANGPO1 61-70F	2.41	-13.97	65	3993	29.41975	88.25762	Stage I
TSANGPO-2A	-2.45	-18.40	60	4057	29.09726	87.59260	weak Stage I
TSANGPO-2B	-2.77	-18.89	60	4057	29.09726	87.59260	weak Stage I
TSANGPO-2C	-2.37	-18.54	60	4057	29.09726	87.59260	weak Stage I
TSANGPO-2D	-1.68	-18.46	60	4057	29.09726	87.59260	weak Stage I
TSANGPO-2E	-1.85	-18.39	60	4057	29.09726	87.59260	weak Stage I
TSANGPO-2F	-3.66	-17.26	60	4057	29.09726	87.59260	weak Stage I
TSANGPO-2G	-1.62	-17.92	60	4057	29.09726	87.59260	weak Stage I
TSANGPO-3A	-6.90	-16.97	100	4455	29.32499	86.92766	weak Stage I
TSANGPO-3B	-5.11	-18.81	100	4455	29.32499	86.92766	weak Stage I
TSANGPO-4(?)A	12.03	-10.09	150	4747	29.48738	86.40288	Stage II
TSANGPO-4(?)B	7.24	-9.83	150	4747	29.48738	86.40288	Stage II
TSANGPO-4(?)C	8.44	-11.91	150	4747	29.48738	86.40288	Stage II
TSANGPO-4(?)D	10.72	-8.76	150	4747	29.48738	86.40288	Stage II
TSANGPO-4 73A	9.88	-10.89	73	4747	29.48738	86.40288	Stage II
TSANGPO-4 73B	9.53	-9.08	73	4747	29.48738	86.40288	Stage II

TABLE 2

(continued)

sample #	δ¹³C (PDB)	δ¹⁸O (PDB)	Depth (cm)	elevation (m)	°N	°E	description*
Tsangpo transect							
TSANGPO-4 73C	9.32	-10.34	73	4747	29.48738	86.40288	Stage II
TSANGPO-4 73D	8.61	-10.08	73	4747	29.48738	86.40288	Stage II
TSANGPO-4 73E	9.79	-11.03	73	4747	29.48738	86.40288	Stage II
TSANGPO-1015 A	-1.83	-11.47	15	4719	30.52402	82.59954	Stage I ?
TSANGPO-10 15B	-1.62	-11.57	15	4719	30.52402	82.59954	Stage I ?
TSANGPO-10 15C	-2.58	-12.53	15	4719	30.52402	82.59954	Stage I ?
TSANGPO-10 15D	-1.00	-11.95	15	4719	30.52402	82.59954	Stage I ?
TSANGPO-10 15E	-2.00	-11.49	15	4719	30.52402	82.59954	Stage I ?
TSANGPO-10 75A	-1.93	-16.27	75	4719	30.52402	82.59954	Stage I ?
TSANGPO-10 75B	-0.37	-14.59	75	4719	30.52402	82.59954	Stage I ?
TSANGPO-10 75C	0.13	-13.91	75	4719	30.52402	82.59954	Stage I ?
TSANGPO-10 75D	-0.83	-14.44	75	4719	30.52402	82.59954	Stage I ?
TSANGPO-11 70A	-4.92	-14.11	70	4719	31.00203	81.14171	weak Stage I
TSANGPO-11 70B	-5.18	-15.27	70	4719	31.00203	81.14171	weak Stage I
TSANGPO-11 70C	-2.98	-17.14	70	4719	31.00203	81.14171	weak Stage I
TSP-12A	-1.07	-15.47	150	3902	29.35858	88.50730	Stage III ps
TSP-12B	-1.17	-15.68	150	3902	29.35858	88.50730	Stage III ps
TSP-13A(A)	-1.32	-16.69	see sample	3969	29.40605	88.25818	Stage I
TSP-13A(b)	4.00	-13.73	see sample	3969	29.40605	88.25818	Stage I
TSP-13A(C)	-0.81	-15.22	see sample	3969	29.40605	88.25818	Stage I
TSP-13B	-1.71	-16.14	see sample	3969	29.40605	88.25818	Stage II ps
TSP-13C	-0.68	-17.24	see sample	3969	29.40605	88.25818	Stage IV ps
TSP-14A	1.00	-17.58	100	3989	29.23353	87.74252	Stage II
TSP-14B	-1.08	-16.09	100	3989	29.23353	87.74252	Stage II
TSP-19A	3.22	-14.08	110	4800	30.41783	82.76712	Stage II/III
TSP-19B	5.81	-9.25	110	4800	30.41783	82.76712	Stage II/III
TSP-19C	3.79	-12.28	110	4800	30.41783	82.76712	Stage II/III
TSP-21A	-2.88	-11.22	60	4016	29.20427	88.30908	Stage II/III
TSP-21B	-0.24	-14.35	60	4016	29.20427	88.30908	Stage II/III
TSP-22A	-2.42	-14.49	55	3854	29.31743	88.94193	Stage I
TSP-22B	-0.13	-16.17	55	3854	29.31743	88.94193	Stage I
TSP-24A	-3.49	-18.24	120	3801	29.35117	89.63483	Stage II
TSP-24B	-1.43	-18.37	120	3801	29.35117	89.63483	Stage II
Zhada Basin region							
TSADA-4A	3.64	-11.91	5	4335	31.37067	79.75019	Stage III-IV
TSADA-4B	-2.10	-13.52	5	4335	31.37067	79.75019	Stage III-IV
TSADA-4C	-1.11	-12.81	5	4335	31.37067	79.75019	Stage III-IV
TSADA-4 2.5A	0.33	-10.53	250	4335	31.37067	79.75019	Stage IV
TSADA-4 2.5B	1.80	-14.95	250	4336	31.37067	79.75019	Stage IV
TSADA-4 2.5C	1.30	-8.43	250	4337	31.37067	79.75019	Stage IV
TSADA-4 2.5D	2.48	-10.33	250	4338	31.37067	79.75019	Stage IV
TSADA-4 2.5E	2.45	-10.60	250	4339	31.37067	79.75019	Stage IV
TSADA-8 UPPTERR/A/	1.46	-15.82	?	3925	31.42349	79.75677	Stage II old
TSADA-8 UPPTERR/B/	5.00	-4.29	?	3925	31.42349	79.75677	Stage II old
TSADA-8 UPPTERR/C/	0.06	-9.58	?	3925	31.42349	79.75677	Stage II old
TSADA-8 UPPTERR/D/	1.97	-10.04	?	3925	31.42349	79.75677	Stage II old
TSADA-8 LOWTERR/	-0.79	-14.41	?	3925	31.42349	79.75677	weak Stage I
TSADA-8 LOWTERR/C	1/.13	-10.05	?	3925	31.42349	79.75677	weak Stage I
TSADA-8 LOWTERR/A	1.24	-4.75	?	3925	31.42349	79.75677	weak Stage I
TSADA-8 LOWTERR/D	0.64	-11.02	?	3925	31.42349	79.75677	weak Stage I
TSANGPO-11 70D	-4.10	-16.47	70	4719	31.00205	81.14173	weak Stage I
TSADA-9 Q3 TERR/A/	3.03	-13.03	110	3920	31.34674	79.78799	Stage II-III
TSADA-9 Q3 TERR/B/	0.71	-15.23	110	3920	31.34674	79.78799	Stage II-III
TSADA-9 Q3 TERR/C/	1.47	-14.42	110	3920	31.34674	79.78799	Stage II-III
TSADA-9 Q3 TERR/D/	1.44	-14.58	110	3920	31.34674	79.78799	Stage II-III
TSADA 11 A	-0.20	-11.36	45	4740	31.47041	80.10346	Stage I

TABLE 2

(continued)

sample #	$\delta^{13}C$ (PDB)	$\delta^{18}O$ (PDB)	Depth (cm)	elevation (m)	°N	°E	description*
Zhada Basin region							
TSADA 11 B	-1.06	-11.97	45	4740	31.47041	80.10346	Stage I
TSADA-11 C	-0.89	-12.51	45	4740	31.47041	80.10346	Stage I
TSADA-12 A	-0.80	-12.57	65	4515	31.49751	80.03679	Stage I
TSADA-12 B	0.08	-12.10	65	4515	31.49751	80.03679	Stage I
TSADA-12 C	-2.07	-12.88	65	4515	31.49751	80.03679	Stage I
TSADA-12 D	-0.67	-12.62	65	4515	31.49751	80.03679	Stage I
TSADA-10 A	-4.36	-11.78	75	4719	31.42809	80.15932	Stage I ?
TSADA-10 b	-3.52	-11.62	75	4719	31.42809	80.15932	Stage I ?
TSADA-10 C	-4.17	-11.98	75	4719	31.42809	80.15932	Stage I ?
TSADA-10D	-4.47	-12.15	75	4719	31.42809	80.15932	Stage I ?
TSADA-10 E	-4.35	-12.50	75	4719	31.42809	80.15932	Stage I ?
TSADA-T1A	3.06	-12.98	65	3676	31.48585	79.71895	Stage I
TSADA-T1B	3.64	-11.56	65	3676	31.48585	79.71895	Stage I
TSADA-15A	5.12	-3.65	0	3676	31.48585	79.71895	stone collar
TSADA-15B	2.31	-9.31	45	3676	31.48585	79.71895	Stage I
TSADA-15C	2.65	-11.09	85	3676	31.48585	79.71895	Stage I
TSADA-T2A	1.32	-10.78	73	3676	31.48573	79.71847	Stage I
TSAD-T2B	1.18	-12.66	73	3676	31.48573	79.71847	Stage I
TSADA-T1Ba	2.90	-5.86	68	3676	31.48585	79.71895	Stage I
TSADA-T1Bb	2.73	-7.55	68	3676	31.48585	79.71895	Stage I
Mount Kailas region							
KAILAO-1 A	-4.93	-14.42	95	4414	31.47884	80.44829	Stage III
KAILAO-1 C	2.10	-3.70	95	4414	31.47884	80.44829	Stage III
KAILAO-1E	-2.92	-11.91	95	4414	31.47884	80.44829	Stage III
KAILAO-1 B	-1.70	-12.55	95	4414	31.47884	80.44829	Stage III
KAILAO-1 D	-1.60	-12.57	95	4414	31.47884	80.44829	Stage III
KAILAO-10 A	7.72	-8.87	5	5370	31.17810	80.99760	Stage I
KAILAO-10 C	9.63	-9.90	5	5370	31.17810	80.99760	Stage I
KAILAO-10 E	7.70	-10.03	5	5370	31.17810	80.99760	Stage I
KAILAO-10 B	10.12	-6.02	5	5370	31.17810	80.99760	Stage I
KAILAO-10 D	10.59	-8.46	5	5370	31.17810	80.99760	Stage I
KAILAO-24 B	-0.15	-11.08	100	4809	31.96970	83.43817	?
KAILAO-24 A	1.45	-12.06	100	4809	31.96970	83.43817	?
KAILAO-24 C	-1.55	-13.06	100	4809	31.96970	83.43817	?
KAILAO-25 A	2.44	-11.54	30	4429	32.11023	83.93373	Stage I
KAILAO-25 C	2.81	-12.03	30	4430	32.11023	83.93373	Stage I
Nema region							
NEMA 1 B	-0.47	-11.59	50	4495	31.77071	87.39829	Stage I
NEMA 1 D	-3.22	-13.38	50	4495	31.77071	87.39829	Stage I
NEMA 1 F	0.09	-11.66	50	4495	31.77071	87.39829	Stage I
NEMA 1 H	-2.50	-13.03	50	4495	31.77071	87.39829	Stage I
NEMA 4 A	-2.72	-13.83	120	4500	31.77035	87.40226	Stage II
NEMA 4 B	7.70	-6.09	120	4500	31.77035	87.40226	Stage II
NEMA 4 C	4.66	-9.12	120	4500	31.77035	87.40226	Stage II
NEMA 4 D	2.33	-10.07	120	4500	31.77035	87.40226	Stage II
NEMA 4 E	-2.01	-13.04	120	4500	31.77035	87.40226	Stage II
NEMA 4 F	-3.39	-13.47	120	4500	31.77035	87.40226	Stage II
NEMA 4 G	-1.84	-12.98	120	4500	31.77035	87.40226	Stage II
NEMA 4 H	-2.47	-13.60	120	4500	31.77035	87.40226	Stage II
Tingri-Rongbuk region							
CP648	1.61	-15.94	-48	4564	28.26642	87.00147	Stage I
CP650	6.31	-10.11	-50	4564	28.26642	87.00147	Stage I
Profile 6							
CP650b	-0.70	-16.20	-50	4564	28.26642	87.00147	Stage I
CP652	-1.14	-15.45	-52	4564	28.26642	87.00147	Stage I
CP654	-2.55	-15.21	-54	4564	28.26642	87.00147	Stage I
CP660	0.49	-15.83	-60	4564	28.26642	87.00147	Stage I

Table 2

(continued)

sample #	$\delta^{13}C$ (PDB)	$\delta^{18}O$ (PDB)	Depth (cm)	elevation (m)	°N	°E	description*
Tingri-Rongbuck region							
CP661	4.21	-12.07	-61	4564	28.26642	87.00147	Stage I
CP664	5.15	-11.13	-64	4564	28.26642	87.00147	Stage I
Profile 8							
CP847	2.92	-18.71	47	4414	28.50633	86.56308	Stage I
CP850	3.67	-19.22	50	4414	28.50633	86.56308	Stage I
CP852	3.03	-18.20	52	4414	28.50633	86.56308	Stage I
CP855	4.15	-17.14	55	4414	28.50633	86.56308	Stage I
CP858	3.74	-18.54	58	4414	28.50633	86.56308	Stage I
CP861	3.95	-17.69	61	4414	28.50633	86.56308	Stage I
CP864	2.91	-19.72	64	4414	28.50633	86.56308	Stage I
CP865	4.39	-17.41	65	4414	28.50633	86.56308	Stage I
CP867	2.87	-19.47	67	4414	28.50633	86.56308	Stage I
CP867b	1.05	-17.18	67	4414	28.50633	86.56308	Stage I
Profile 1							
CP150	3.23	-8.03	50	4205	28.32397	86.04106	Stage I
CP150	2.60	-8.45	50	4205	28.32397	86.04106	Stage I
CP158	6.92	-6.81	58	4205	28.32397	86.04106	Stage I
CP158	7.23	-6.47	58	4205	28.32397	86.04106	Stage I
CP188	-6.44	-17.40	88	4205	28.32397	86.04106	Stage I
CP188	-6.71	-15.93	88	4205	28.32397	86.04106	Stage I
Profile 5							
CP550	-4.33	-18.37	50	4517	28.27492	87.01772	Stage I
CP560	-3.73	-16.91	60	4517	28.27492	87.01772	Stage I
CP560	1.29	-15.51	60	4517	28.27492	87.01772	Stage I
Profile EB							
EBC50	4.59	-19.06	50	5200	28.14100	86.85072	Stage I
EBC50pure	3.71	-19.38	50	5200	28.14100	86.85072	Stage I
EBC501.1	5.05	-18.88	50	5200	28.14100	86.85072	Stage I
Profile 4							
CP428	-4.10	-14.19	28	4825	28.25561	87.08383	Stage I
CP430	-3.93	-14.74	30	4825	28.25561	87.08383	Stage I
CP432	-3.41	-13.80	32	4825	28.25561	87.08383	Stage I
CP438	-5.02	-15.14	38	4825	28.25561	87.08383	Stage I
CP439	-4.62	-15.31	39	4825	28.25561	87.08383	Stage I
CP445	-3.02	-12.66	45	4825	28.25561	87.08383	Stage I
CP446	-2.64	-14.18	46	4825	28.25561	87.08383	Stage I
CP455	-4.24	-16.15	55	4825	28.25561	87.08383	Stage I
CP452	-3.03	-13.87	52	4825	28.25561	87.08383	Stage I
CP458	-1.83	-12.67	58	4825	28.25561	87.08383	Stage I
CP460	-3.13	-13.99	60	4825	28.25561	87.08383	Stage I
CP465	-5.88	-16.01	65	4825	28.25561	87.08383	Stage I
CP467verypure	-4.77	-16.52	67	4825	28.25561	87.08383	Stage I
CP475	-6.04	-15.98	75	4825	28.25561	87.08383	Stage I
CP477	-5.72	-15.43	77	4825	28.25561	87.08383	Stage I
CP480	-4.15	-12.90	80	4825	28.25561	87.08383	Stage I
Profile 3							
CP305	0.55	-7.90	5	3741	28.28500	87.38472	Stage I
CP35-7	1.27	-8.71	6	3741	28.28500	87.38472	Stage I
CP307	2.07	-5.72	7	3741	28.28500	87.38472	Stage I
CP309	0.60	-8.03	9	3741	28.28500	87.38472	Stage I
CP310	0.53	-9.97	10	3741	28.28500	87.38472	Stage I
CP311	-0.07	-10.28	11	3741	28.28500	87.38472	Stage I
CP312	0.09	-9.24	12	3741	28.28500	87.38472	Stage I
CP319	-1.13	-14.69	19	3741	28.28500	87.38472	Stage I
CP321pure	-1.59	-14.58	21	3741	28.28500	87.38472	Stage I
CP325pure	-0.69	-14.47	25	3741	28.28500	87.38472	Stage I
CP331pure	-1.11	-15.09	31	3741	28.28500	87.38472	Stage I

TABLE 2

(continued)

sample #	δ¹³C (PDB)	δ¹⁸O (PDB)	Depth (cm)	elevation (m)	°N	°E	description*
Tingri-Rongbuck region							
Profile 3							
CP336	0.25	-16.39	36	3741	28.28500	87.38472	Stage I
CP345	-0.08	-17.30	45	3741	28.28500	87.38472	Stage I
CP346	0.39	-18.13	46	3741	28.28500	87.38472	Stage I
CP349	0.68	-17.35	49	3741	28.28500	87.38472	Stage I
CP351	-1.67	-16.63	51	3741	28.28500	87.38472	Stage I
CP365	1.37	-17.11	65	3741	28.28500	87.38472	Stage I
CP365	1.50	-17.09	65	3741	28.28500	87.38472	Stage I
CP365-66			66	3741	28.28500	87.38472	Stage I
CP368	1.60	-17.08	68	3741	28.28500	87.38472	Stage I
CP373	0.15	-16.72	73	3741	28.28500	87.38472	Stage I
CP374	0.91	-17.40	74	3741	28.28500	87.38472	Stage I
north India soils							
INACR-11A	-0.47	-6.07	175	233	29.73858	76.97270	Stage II
INACR-11B	-0.61	-5.97	175	233	29.73858	76.97270	Stage II
INACR-11C	-0.51	-6.16	175	233	29.73858	76.97270	Stage II
INACR-50A	-3.28	-6.29	85	348	32.58407	74.99010	Stage I-II
INACR-50B	1.53	-5.61	85	348	32.58407	74.99010	Stage I-II
INACR-50C	-3.52	-6.20	85	348	32.58407	74.99010	Stage I-II
INACR-53A	-3.62	-6.12	50	189	31.12400	74.95065	Stage I
INACR-53C	2.11	-5.03	50	189	31.12400	74.95065	Stage I
INACR-57A	-3.03	-5.54	200	340	27.19735	74.30608	Stage II
INACR-57B	-2.88	-5.42	200	340	27.19735	74.30608	Stage II
INACR-58A	2.07	-4.28	60	343	27.38020	74.54048	Stage I
INACR-58B	2.16	-3.65	60	343	27.38020	74.54048	Stage I
INACR-58C	2.21	-2.69	60	343	27.38020	74.54048	Stage I
INACR-59A 300	-3.37	-5.02	175	495	27.37607	75.82045	Stage I
INACR-59B 300	-0.93	-4.32	175	495	27.37607	75.82045	Stage I
INACR-60A(b)	-0.96	-5.71	80	417	27.17663	75.45528	Stage I
INACR-60A(c)	-0.93	-5.65	80	417	27.17663	75.45528	Stage I
Ngangla Ringsto-							
lacustrine tufa							
NRC10-86-1b	5.66	-4.79	NA	4775	31.63266	82.65086	shoreline tufa
NRC10-98-1	1.94	-4.12	NA	4737	31.608314	82.82877	shoreline tufa
NRC10-100-1	4.97	-2.90	NA	4762	31.605916	82.832077	shoreline tufa
NRC10-101 BTM	3.83	-4.79	NA	4752	31.605476	82.832402	shoreline tufa

* Stage (I-IV) refers to stage of carbonate development, after Gile and others (1966). See text for discussion.

*Transect studies from Bhotse Khola and Tingri-Rongbuk.*—In one Holocene soil (CP3) from the Tingri-Rongbuck area, carbonate clast coatings were obtained from 5 to 80 cm depth. The δ¹⁸O values of carbonate clast coatings in this soil decrease with depth in a concave-down profile that is characteristic of *in situ,* modern pedogenic carbonate profiles observed in previous studies (fig. 9; Quade and others, 1989a; Breecker and others, 2009). Pedogenic carbonates from soil CP3 have relatively high δ¹⁸O values that decrease abruptly with depth in the shallow subsurface but are restricted to a narrow range of relatively low δ¹⁸O values below 40 cm depth. The shape of the carbonate profile in soil CP3 justifies why we distinguish in this study between carbonate sampled above and below 50 cm soil depth. The δ¹⁸O values of carbonates formed at depths shallower than 40 to 50 cm are likely to have been influenced by the evaporation of soil water.

TABLE 3

"Clumped isotope" data and modeled site temperature

sample	latitude	longitude	Elevation (m)	sample depth (cm)	Stage*	δ¹³C (PDB)	δ¹⁸O (PDB)	Δ₄₇	±	Δ₄₈	±	Δ₄₇-based T (°C)	±	mean annual T (°C)	maximum monthly T (°C)	modeled maximum T (°C) at sample depth
L-4a	N29°37′18.8″	E88°56′51.6″	3809	58±12	II-III	-1.80	12.43	0.6821	0.0087	1.704	0.226	17.22	1.8	4.73	14.23	11
L-4b	N29°37′18.8″	E88°56′51.6″	3809	58±12	II-III	-2.08	12.32	0.6757	0.0092	0.97	0.229	18.57	1.92	4.73	14.23	11
TSP-19a	N30°2′57.8″	E82°4′62.7″	4800	110±12	II	3.23	16.28	0.71	0.0085	0.554	0.207	11.63	1.65	-3.70	8.68	1
TSP-19b	N30°2′57.8″	E82°4′62.7″	4800	110±12	II	7.30	18.79	0.7141	0.0085	1.215	0.192	10.83	1.64	-3.70	8.68	1
TSP-21Ba	N29°1′22.5.6″	E88°1′8′54.5″	4016	50±5	II	-4.39	11.46	0.6527	0.0088	1.663	0.231	23.5	1.94	2.97	13.07	10
TSP-21Bb	N29°1′22.5.6″	E88°1′8′54.5″	4016	50±5	II	-4.47	11.07	0.6616	0.0094	1.524	0.241	21.56	2.03	2.97	13.07	10
TSP-21Bc	N29°1′22.5.6″	E88°1′8′54.5″	4016	50±5	II	-4.20	11.26	0.6418	0.0085	3.56	0.225	25.95	1.93	2.97	13.07	10
TSP-22a	N29°1′94.6″	E88°56′51.6″	3876	60±10	II-III	0.27	11.87	0.6605	0.0085	0.216	0.235	21.8	1.83	4.16	13.85	10.5
TSP-22b	N29°1′94.6″	E88°56′51.6″	3876	60±10	II-III	0.30	12.03	0.6797	0.0081	1.147	0.233	17.72	1.68	4.16	13.85	10.5

* Stage (I-IV) refers to stage of carbonate development, after Gile and others (1966). See text for discussion.
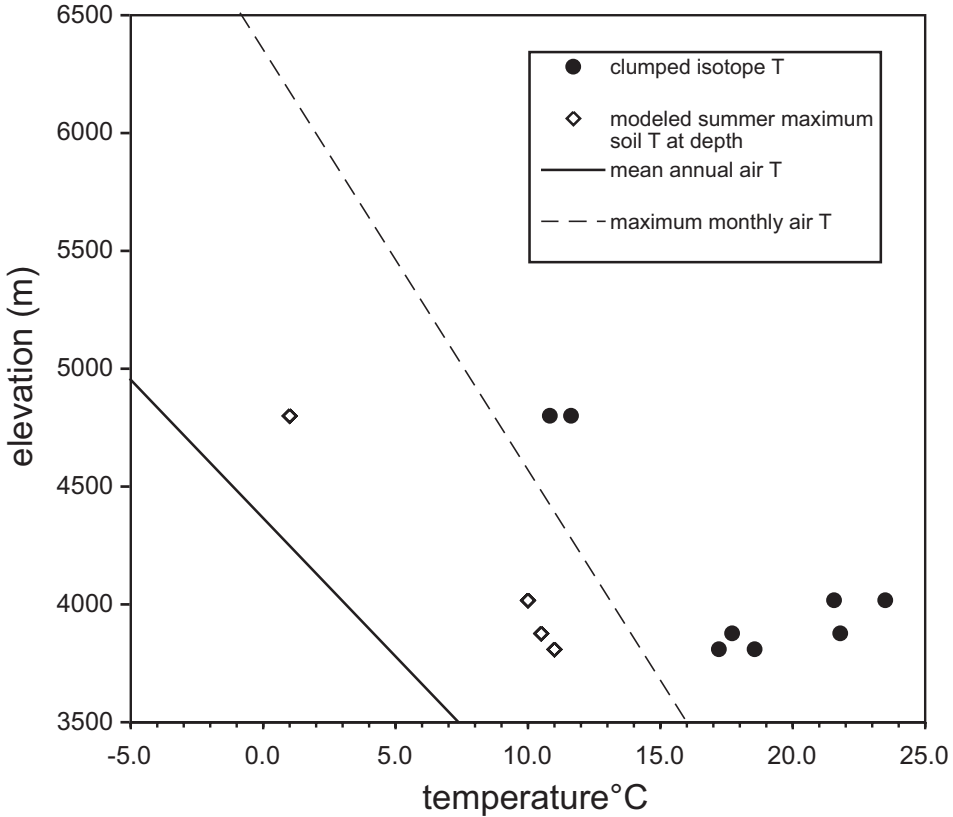
Fig. 8. Temperature estimates of carbonate formation for southern Tibet from clumped-isotope analyses compared to elevation gradients of mean annual and maximum monthly air temperature, and to modeled summer maximum soil temperature at the relevant depth of carbonate formation (see table 3).

Assuming isotopic equilibrium, we can calculate the $\delta^{18}O_{cc}$ values from $\delta^{18}O_{mw}$ values throughout our paper using the relationship from Kim and O'Neil (1997). The $\delta^{18}O_{mw}$ values calculated from $\delta^{18}O_{cc}$ values and their corresponding elevations can be compared with the modern $\delta^{18}O_{mw}$-elevation relationship for the Himalayas (fig. 4). Ice records from Tibetan Plateau (fig. 1) suggest that the $\delta^{18}O_{mw}$ values prior to 1800 A.D. were ~2 permil lower than they are today (Thompson and others, 2003). To accurately compare late Holocene carbonate with modern meteoric water, a correction of 2 permil was added to each calculated $\delta^{18}O_{mw}$ value. At each elevation, the calculated $\delta^{18}O_{mw}$ values are lower than measured modern values if mean annual air temperatures are used. However, using soil temperatures equal to MAT+15 °C, which approximates the temperature of carbonate formation in Tibetan soils according to the clumped isotope measurements, shifts the calculated $\delta^{18}O_{mw}$ values into better agreement with modern meteoric water (fig. 4). We measured soil temperatures at 50 cm depth in June and July that were ~12 °C higher (table 4) than estimated mean annual air temperature, indicating MAT+15 °C is entirely reasonable for carbonate formation. The agreement between measured and calculated $\delta^{18}O_{mw}$ values suggests pedogenic carbonate does reliably record the $\delta^{18}O$ value of local meteoric water, but that carbonate does not form at mean annual temperature. Instead soil carbonate forms in oxygen isotope equilibrium with soil water during the late spring/early
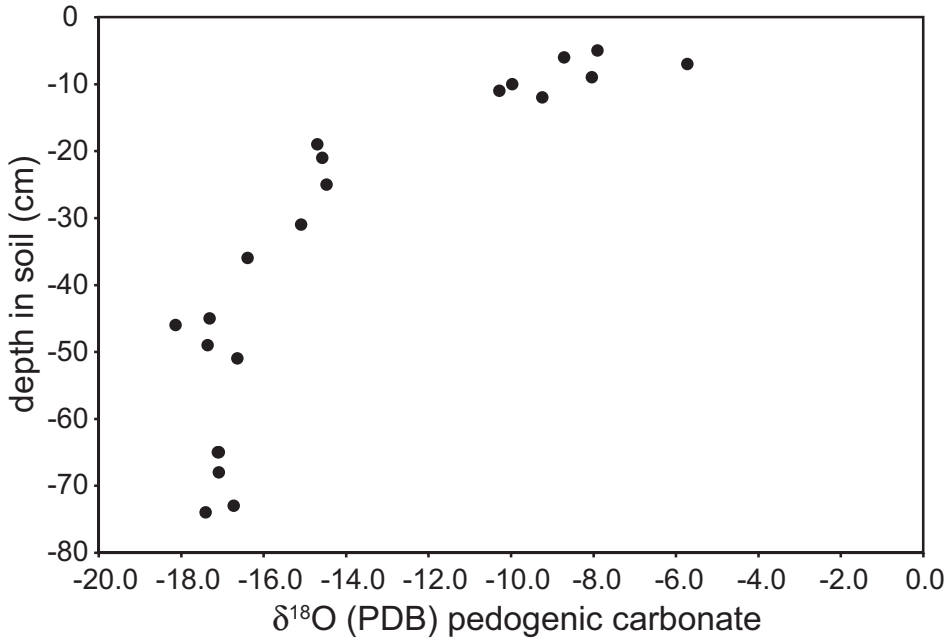
Fig. 9. $\delta^{18}O$ (PDB) values of soil carbonate with sample depth from a terrace profile CP3 (3741 m) in the Tingri-Rongbuk area of southern Tibet. See table 2.

summer, when soil temperatures are much higher than mean annual air temperature, consistent with the observations of Breecker and others, (2009). The magnitude of elevation overestimates associated with using MAT rather than MAT+15 °C to calculate $\delta^{18}O_{mw}$ values from measured $\delta^{18}O_{cc}$ values is 500 to 800 meters (fig. 10).

Observed differences of 15 °C between mean annual air and summer soil temperature exceed those reported for Africa (Passey and others, 2010) and for South America (Hoke and others, 2009) by 5 to 10 °C. We believe the differences are real and reflect the lack of shading vegetation on our Tibet sites and of rain to cool soils in June, the hottest month on the plateau.

TABLE 4

Measured and estimated mean annual air temperature, Tingri-Rongbuk soil sites

soil site	elevation (m)	mean annual T (°C)*	measured June T (°C)	June T minus MAT
CP3	3741	5.3	13.0	7.7
CP4	4825	-3.7	9.3	13.0
CP5	4517	-1.0	9.1	10.1
CP6	4564	-1.4	13.7	15.1
CP8	4414	-0.1	15.5	15.6
			average difference:	12.3

* Calculated from equation 1 in text.
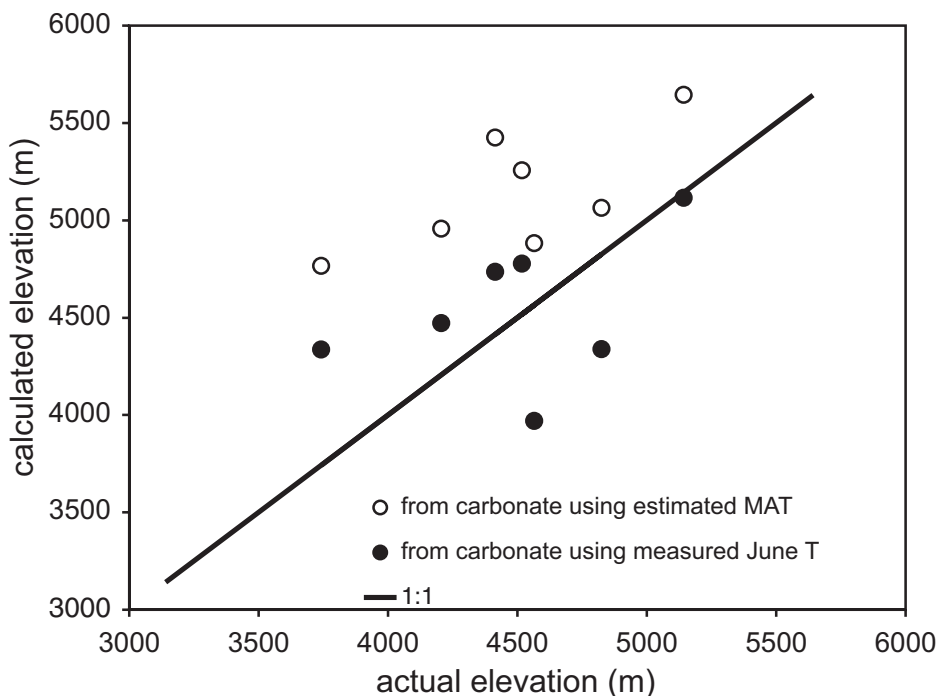
Fig. 10. Actual sample site elevations versus elevation calculated from the local $\delta^{18}O$ (PDB) value of soil carbonate for the Tingri-Rongbuk area (fig. 1; table 2). Assuming warm June temperatures (filled circles; average MAT+13 °C) of carbonate formation rather than mean annual temperature (open circles) produces a much better fit of calculated to observed elevation.

Our temperature observations from the Tingri-Rongbuk area and the agreement of observed (here and in Garzione and others, 2000a) and modeled (Rowley and others, 2001) $\delta^{18}O_{mw}$ values allow us to formulate the $\delta^{18}O_{cc}$ value-elevation (in masl) relationship for the Himalayan front as:

$$elevation\,(masl) = -7x10^{-11}(\delta^{18}O_{cc})^3 + 4x10^{-7}(\delta^{18}O_{cc})^2 - 0.0015(\delta^{18}O_{cc}) - 10.067 \quad (5)$$

Here we use the $\delta^{18}O_{mw}$-elevation relationship of equation 6 from Rowley and others (2001), and assume T°C=MAT+15 °C, where T°C is calculated from equation (1).

Regional patterns in Tibet.—There is a very clear pattern of decrease of $\delta^{18}O_{cc}$ values from lowland India up to the Himalayan crest (table 2). Modern soils in north India average around −5 permil on the Gangetic plain and decrease to −15 to −19 permil at the highest elevations at Tingri-Rongbuk. Soils in the intervening 500 to 3000 masl are non-calcareous due to the wet monsoonal climate.

Northward across the Tibetan Plateau there is a very large scatter in $\delta^{18}O_{cc}$ values with latitude from sampling depths below and above 50 cm. On the other hand, the most negative $\delta^{18}O_{cc}$ values increase northwards, the same pattern seen in $\delta^{18}O_{mw}$ values. There is no correlation of $\delta^{18}O_{cc}$ with longitude or with elevation detrended for latitude (fig. 11).

Hence, the same picture emerges from $\delta^{18}O_{cc}$ and $\delta^{18}O_{mw}$ values across southern Tibet, even after some adjustment for evaporation effects by selecting for samples from >50 cm depth. The lack of a correlation with elevation may again be probably caused by the greater proportion of winter-westerly rainfall at higher elevations (Tian and
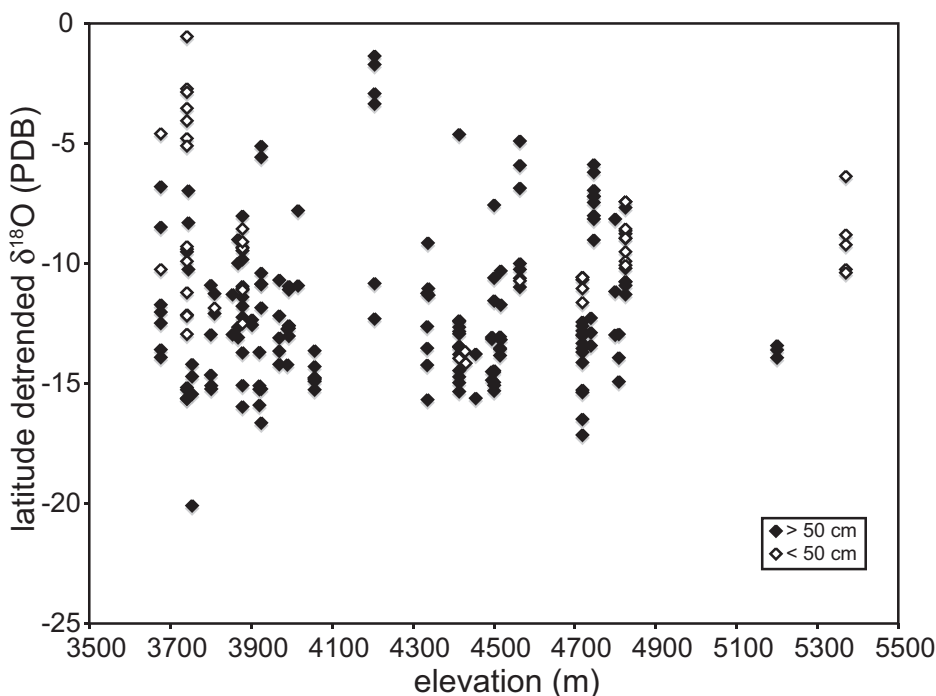
Fig. 11. Latitude-detrended $\delta^{18}O$ (PDB) value of soil carbonate on the Tibetan Plateau versus sampling elevation.

others, 2007) accentuated by lower soil temperatures at higher elevations (countering cloud-mass distillation effects).

The relationship on the plateau between $\delta^{18}O_{cc}$ and $\delta^{18}O_{mw}$ values is largely supported by empirical carbonate/water/temperature data from Bhotse Khola and Tingri-Rongbuk, and we can see from figure 12 that it accounts for all but the lowest values in the regional data set on the plateau. We attribute the modest mismatch of $\delta^{18}O_{cc}$ values between the theoretical values compared to those from our regional data set to even warmer temperatures than the MAP+15 °C assumed, or to stronger monsoonal rainfall during the 10^5 year span archived in some soils. Monsoon rainfall across probably varies on precessional time scales (~23 kyr periodicity) in southern Tibet, which is currently experiencing an insolation minimum following a maximum in insolation about 10 ka. With higher insolation, rainfall increased, as evidenced by the dramatic growth of lakes across Tibet in the early Holocene (for example Gasse and others, 1996; Mügler and others, 2010). Due to the Amount Effect (Rozanski and others, 1993; Zhang and others, 2002), more rainfall during strong monsoon periods should decrease $\delta^{18}O_{cc}$ values. Therefore, the very negative $\delta^{18}O_{cc}$ values in our regional data set not explained by modern $\delta^{18}O_{mw}$ values and summer temperatures may have developed under wetter monsoonal conditions in the past.

Lacustrine carbonates.—We analyzed lacustrine tufa encrusting paleoshorelines around paleolake Ngangla Ringsto central Tibet (fig. 1). Although not strictly modern, these deposits are mid-Holocene age and formed near the current elevation of the lake, and therefore provide some insight into recent isotopic patterns in Tibetan lakes. $\delta^{18}O$ values of the fossil tufa (table 2: −5 to −2.9‰ in PDB) and modern lake water (table 1: −3.7‰ in SMOW) are high, reflecting strong evaporation of lake water.
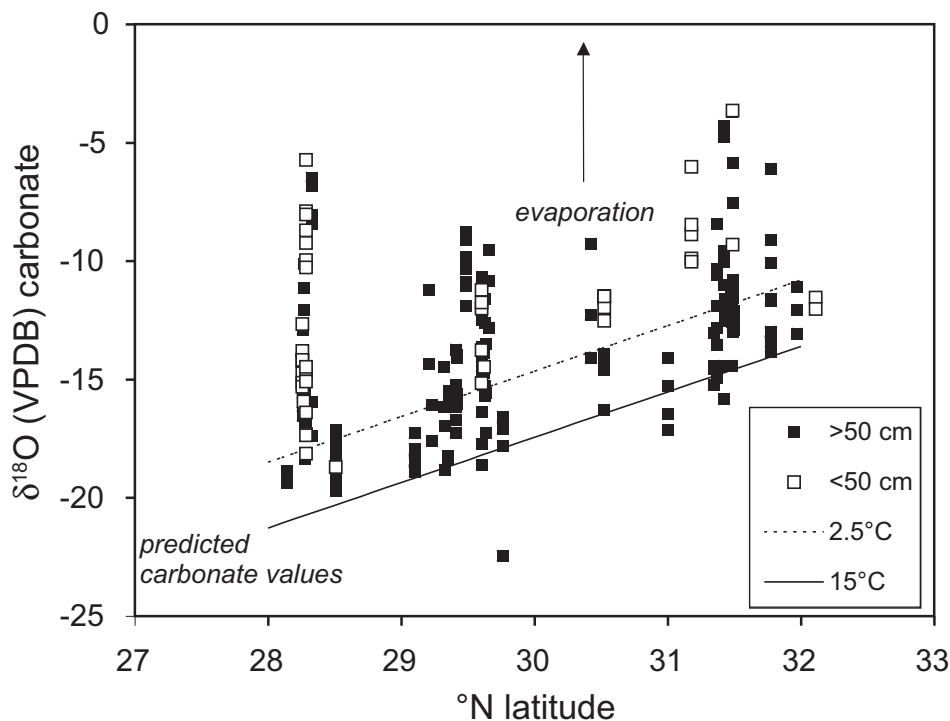
Fig. 12. The observed $\delta^{18}O$ (PDB) values of surficial soil carbonate (from >50 and <50 cm soil depth) in Tibet versus $\delta^{18}O$ (PDB) values predicted from 2004–2006 stream waters using the regression equation in figure 5A, at soil temperatures of 2.5 and 15 °C.

Comparing the two, we arrive at estimates of formation temperatures in the 10 to 19 °C range, well above mean annual temperature of $\sim$ -2 °C. Diurnal temperatures of surface water measured by us ranged between about 6 and 12 °C in June, the warmest month on the plateau. These summer water temperatures therefore exceed mean annual temperatures at this site by 8 to 14 °C. Preferential growth of lake carbonates in the summer half year when biologic activity is at its peak has been suggested by other studies (Huntington and others, 2009). Based on our admittedly meager modern lake data from Tibet, we tentatively adopt formation temperature estimates for shallow lake carbonates (tufa, shell, marl) of MAT+15 °C, similar to that for soil carbonates.

EVALUATION OF THE ISOTOPIC RECORD OF ELEVATION CHANGE

Paleoaltimetry in Tibet has been approached from a variety of perspectives, including the use of geodynamic, tectonic, volcanic, and paleobotanic evidence. Paleoelevation reconstruction in Tibet using stable isotopes only commenced in 2000 with the study of Garzione and others (2000a, 2000b). At least eleven more studies have followed since then, eight on the plateau (Rowley and others, 2001; Currie and others, 2005; Cyr and others, 2005; Rowley and Currie, 2006; Wang and others, 2006; DeCelles and others, 2007; Polissar and others, 2009; Saylor and others, 2009), and three just beyond its northern fringes (Dettman and others, 2003; Graham and others, 2005; and Kent-Corson and others, 2009). Of these we will confine our attention to the studies from the plateau itself to which thermodynamic and empirical models of isotopic distillation can be applied to reconstruct paleoelevation. The distribution of studies is

sparse when one considers the probable duration of elevation change, Eocene to present, and the plateau's huge extent, an area roughly the size of the western USA. In this sense, our summary constitutes a very early progress report.

There are a variety of issues attending any paleoelevation reconstruction, such as age control, diagenesis, sample type, evaporation effects, assumed paleotemperatures, and climate change effects. In our re-examination of the records, we will leave aside the issue of diagenesis and age control and focus on the remaining items on the list. In passing we would point out that diagenetic resetting is a major concern for isotopic reconstructions of paleoelevation, especially in deep time, and difficult to disprove completely despite the efforts by us and others (for example Garzione and others, 2004; DeCelles and others, 2007; Saylor and others, 2009; and Leier and others, 2009).

Soil carbonate, aquatic shell and marl have been the main focus of paleoaltitude reconstruction on the Tibetan Plateau. Special considerations attend the use of each type. Firstly, soil carbonate precipitates *in situ* from rainwater falling directly on the site, whereas aquatic marl and shell precipitate in lakes and rivers fed by higher elevation run-off. As such, the isotopic composition of soil carbonate reflects local elevation, whereas that of aquatic shell and carbonate record elevations of the surrounding paleocatchment. Thus, in the case of the Xol Xil, middle Niubao, Dingqing, Zhada, and parts of Nima and Thakkola studies, the reconstructed paleoelevations pertain to the catchment surrounding the paleobasin. For the upper Nuibao, Namling, and some of Nima and Thakkola, paleosol carbonate was sampled, and thus local basin paleoelevation is being reconstructed.

For all these materials, evaporation can drastically enrich ^{18}O in host water, producing large underestimates in paleoelevation. In soils, the best approach is to sample carbonate as repeatedly and deeply (>50 cm) in the paleoprofile as possible, and then choose only the lowest δ^{18}O values for interpretation. Evaporation effects with aquatic shell depend critically on the nature of the host water. For example, Saylor and others (2009), analyzing fossil shell from the Mio-Pliocene Zhada Formation, documented major enrichment in ^{18}O in lacustrine mollusks and more modest enrichments in paludal mollusks, all in comparison to mollusks from fluvial deposits. These patterns match patterns in δ^{18}O values of modern Tibetan waters. The difference between the riverine and lacustrine taxa was ~10 permil, equivalent to a ~4 km underestimate of paleoelevation using the δ^{18}O values from the lacustrine carbonates! The absence of an evaporative signal in modern soil water and stream water measured as part of this study show that paleosol carbonate >50 cm and mollusk shells from fluvial deposits should provide the most accurate isotopic records of paleoelevation.

Paleo-temperature has to be assumed in order to reconstruct δ^{18}O$_{mw}$ values from δ^{18}O$_{cc}$ values. Fortunately, reconstructed δ^{18}O$_{mw}$ values are not very sensitive to temperature uncertainties: a ±10 °C uncertainty translates into ±2 permil, or about ±770 m. Most previous isotopic studies on the plateau, including our own, have assumed paleotemperatures of 5 to 10 °C, slightly higher than mean annual air temperatures today at 4500 m, with an error of ±5 to 10 °C. Our results suggest that the relevant temperatures of formation in soils are 10 to 15 °C above local mean annual temperature. Although less well studied, this appears to also be the case for lakes, where biological activity will be focused in the warmest part of the summer half-year. We therefore assumed formation temperatures of 20 ± 8 °C for all lake and soil carbonates, which we suggest encompasses the temperature range of most lakes and soils during the summer season of carbonate formation across 0 to 5000 masl for Tibet. The ±8 °C uncertainty accounts for most of the ±1000 m uncertainty of our paleoelevation estimates shown in figure 7. Once better calibrated for modern Tibetan soils and lakes, Δ_{47}-based temperatures should further reduce our uncertainties in

paleotemperatures and provide an independent (entirely temperature-based) estimate of paleoelevation.

The issue of climate change is probably the biggest challenge facing paleoelevation reconstruction on the plateau. Correction for this issue has been addressed by Rowley and others (2001) by use of the term $\Delta\delta^{18}O_p$, defined as: $\Delta\delta^{18}O_p = \delta^{18}O_p - \Delta\delta^{18}O_o$, where $\delta^{18}O_{paleomw}$ denotes the reconstructed value of paleowater at some unknown paleoelevation, and $\delta^{18}O_o$ is the assumed value for paleowater at sea-level in the moisture source region. The concept is that subtraction of the source term corrects for any change other than elevation that might modify $\delta^{18}O$ values throughout the region, such as global temperature changes, continental drift, or the $\delta^{18}O$ value of the ocean. Paleoelevation can thereby be calculated from the equation of Rowley and others (2001) in our equation 6 below:

elevation (*masl*)

$$= -6.14x10^{-3}(\Delta\delta^{18}O_p)^4 - 0.6765(\Delta\delta^{18}O_p)^3 - 28.623(\Delta\delta^{18}O_p)^2 - 650.66(\Delta\delta^{18}O_p) \quad (6)$$

in which we redefine $\Delta\delta^{18}O_p$ as:

$$\Delta\delta^{18}O_p = \delta^{18}O_p - 1.5 \times (°N \text{ of Himalayan crest}) - \delta^{18}O_o.$$

This modification compensates for the northward decrease in $\delta^{18}O_{mw}$ values observed on the Tibetan Plateau today.

Since Indo-Asian collision in the Early Tertiary, $\delta^{18}O_o$ certainly changed through time in response to changes in the isotopic composition of the ocean (Zachos, 1994), to global temperature (Lear and others, 2000), and to the 10 to 15° northward drift of southern Tibet. There are both empirical and theoretical approaches to estimating these changes in $\delta^{18}O_o$. The empirical approach uses the $\delta^{18}O_{cc}$ value from paleosols in the low-elevation Himalayan foreland to calculate $\delta^{18}O_o$ (Rowley and others, 2001a; Quade and others, 2007; Saylor and others, 2009). The limitation here is that the paleosol record only extends back to about 17 Ma. Moreover, it is debatable how much of the ~3 permil shift in $\delta^{18}O_{cc}$ values it displays over the past 17 Ma reflects a shift in $\delta^{18}O_{mw}$ (Quade and others, 1989b; Quade and others, 2007), versus the influence of local soil evaporation.

For the theoretical approach, Rowley and Garzione (2007) assumed that ±3 permil variation around an assumed long-term average $\delta^{18}O_o$ value of −3 permil accounted for all the changes over the past 50 Ma. −3±3 permil brackets the $\delta^{18}O_{mw}$ value of mean weighted rainfall of −5.81 permil from New Delhi today. For our paper we modeled these combined effects through time on $\delta^{18}O_o$ (fig. 13), which is observed to change very little from modern values, due mainly to the offsetting effects of northward drift in Tibet (reducing $\delta^{18}O_o$) versus global cooling and ice cap build-up (increasing $\delta^{18}O_o$).

The limitation of the theoretical approach is that we don't know how to account for changes in the strength of the Asian Monsoon. We have already noted that increases in the intensity of the monsoon on precessional timescales during just the Quaternary probably have altered average $\delta^{18}O_{mw}$ value of precipitation on the plateau. For the longer term this is a key unknown. Suffice it to say, a weaker monsoon in the deeper geologic past would very likely produce lower isotope-elevation gradients, as well as reduce penetration of monsoonal rainfall northward. This would produce higher $\delta^{18}O_{mw}$ values for a given elevation, and therefore lead to underestimates of true paleoelevation using the lapse rates currently assumed by all of us, and using the modern latitudinal isotopic gradient across the plateau assumed in this paper.
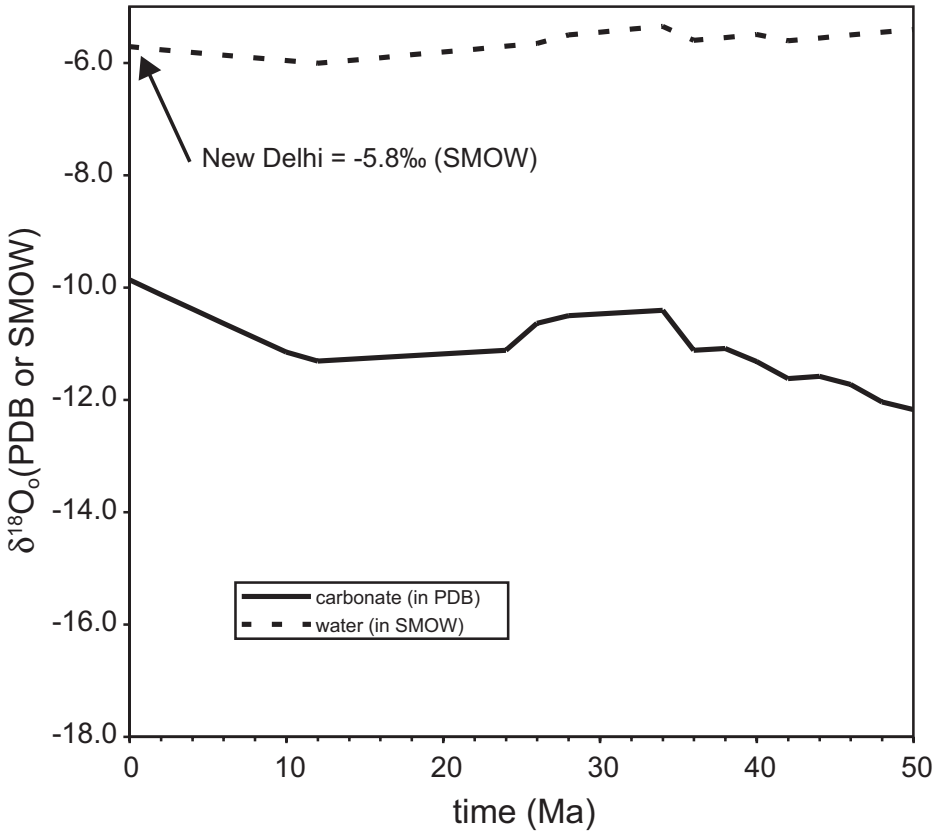
Fig. 13. Modeled evolution through time of $\delta^{18}O_o$, the value for north Indian rainfall (expressed in SMOW), compared to the $\delta^{18}O_{cc}$ value (expressed in PDB) of low-elevation soil carbonate. Over the past 50 Ma, the model assumes at ~14 °C drop in soil temperature, northward drift of India by 10°, and a roughly 1‰ increase in the $\delta^{18}O$ value of sea-water due to ice build-up.

We can now compare our revised estimates of paleoelevation, using equation 6 (fig. 7A), to the estimates from previous studies. Thus far, all studies conclude that the southern Tibetan Plateau encompassing all of the Lhasa Terrane has been at elevations similar to—and in one case (Saylor and others, 2009) greater than—today since the late Eocene. North of the Lhasa Terrane, there is only one study available, from Xoh Xil located at about 36 °N, within the Songpan-Ganzi flysch complex (fig. 1; Cyr and others, 2005). The conclusion of that study is the region was much lower than its current 4.7 km elevation, at ~2 km in the late Eocene. From this Rowley and Currie (2006) suggested that southern Tibet stood at elevations comparable to today shortly after collision, but that central and northern Tibet rose later, as collision propagated and India underthrusted northward.

With the exception of Xoh Xil, our reconstructions largely agree with previous reconstructions: there is no evidence that the elevation of the Tibetan Plateau has changed by more than ±500 to 1000 masl since the middle Eocene. At sites well north of the Himalayan crest such as Nima (26 Ma), our higher estimated paleotemperatures (compared to those used by previous studies) partially offset the effects of latitude, and so we arrive at the similar paleoelevation reconstructions as previous studies but for different reasons. At Thakkola (11 Ma), and Zhada (2-9 Ma) next to the Himalayan

crest, paleoelevations appear to have been higher by ~1 km (see Saylor and others, 2009 for in depth discussion of the Zhada case), although these estimates lie near the limits of the probable error on the analysis. In the case of Xoh Xil, we place the basin catchment closer to 4 km, rather than the ~2 km of Cyr and others (2005), by accounting for its position 6.6° north of the Himalayan crest. This consideration, as well as modest changes in $\delta^{18}O_o$, increases the reconstructed paleoelevation of Xoh Xil to within ~ one kilometer of its current elevation. The plateau north of Xoh Xil remains unstudied. However, evidence described by Kent-Corson and others (2009) on the northern flank of the plateau point to gradual aridification of the area starting in the early Neogene, perhaps due to withdrawal of marine waters and local uplift. This would support the hypothesis of Molnar and Stock (2009) that the northernmost plateau rose more recently than the center and southern plateau.

In summary, our reevaluation of the admittedly very scanty isotopic evidence suggests that large areas of southern and central Tibetan Plateau stood close to their current high elevations at the time of or shortly after Indo-Asian collision. Much of this high elevation could have been inherited from orogeny pre-dating Indo-Asian collision. For example, Murphy and others (1997), Kapp and others (2007), and Volkmer and others (2007) present evidence for extensive compressional deformation and shortening prior to Indo-Asian collision of the Lhasa Terrane, suggesting the presence of an Andean-style Altiplano (the "Lhasaplano"). The other terranes that compose the plateau, such as the Qiangtang Terrane, also experienced significant pre-Tertiary deformation (Kapp and others, 2005), and were probably elevated by their collision with Asia during the Mesozoic, by compressional deformation during the subsequent subduction of Neotethyan oceanic crust, and lastly by Lhasa Terrace docking in the early Cretaceous. Future paleoaltimetric studies targeting Mesozoic rocks in the Qiangtang and Songpan-Ganzi terranes will undoubtedly test this possibility.

<div align="center">CONCLUSIONS</div>

Our paper seeks to improve paleoelevation estimates on the Tibetan Plateau by grounding them in a detailed consideration of the modern isotopic and climatic patterns in the region. Our extensive modern data set supports previously determined empirical (Garzione and others, 2000a) and theoretical (Rowley and others, 2001) isotope-elevation gradients for the Himalayan front. Our results also verify the original observations of Tian and others (2001) and Zhang and others (2002) that $\delta^{18}O_{mw}$ values decrease gradually north of the Himalayan crest, a reflection of the diminishing contribution of summer monsoon rainfall northward. Moreover, our analysis of Δ_{47} and $\delta^{18}O$ values in modern soil carbonate strongly suggests that carbonates form at ≥ 10 °C higher than mean annual temperature, a hypothesis that will require further testing by direct temperature observations in modern soils.

We recalculated paleoelevations from six previous studies on the plateau, incorporating the effect of position north of the Himalayan crest as well as higher assumed (MAT+15 °C) temperatures of formation. The result largely supports the conclusions of previous reconstructions, including the possibility of paleoelevations (Saylor and others, 2009) even higher than today in southern Tibet during the Mio-Pliocene. The one notable exception is the reconstructed paleoelevation for Hoh Xil in north-central Tibet, which for the late Eocene we place much closer to it's current high elevation than previous reconstructions (Cyr and others, 2005; Rowley and Currie, 2006). In our view, a robust test of the various geodynamic models of elevation change awaits expansion and replication of isotopic records all across Tibet, with particular emphasis on the center and north and for the period >15 Ma.

REFERENCES

Affek, H. P., Bar-Mathews, M., Ayaalon, A., Mathews, A., and Eiler, J. M., 2008, Glacial/interglacial temperature variations in Soreq cave speoaloethems as recorded by "clumped isotope" thermometry: Geochimica et Cosmochimica Acta, v. 72, p. 5351–5360, doi:10.1016/j.gca.2008.06.031.
Bartlett, M. G., Chapman, D. S., and Harris, R. N., 2006, A decade of ground-air temperature tracking at Emigrant Pass Observatory, Utah: Journal of Climatology, v. 19, p. 3722–3731, doi:10.1175/JCLI3808.1.
Blisniuk, P. M., and Stern, L. A., 2005, Stable isotope paleoaltimetry: A critical review: American Journal of Science, v. 305, p. 1033–1074, doi:10.2475/ajs.305.10.1033.
Bookhagen, B., Fleitmann, D., Nishiizumi, K., Strecker, M. R., and Thiede, R. C., 2006, Holocene monsoonal dynamics and fluvial terrace formation in the northwest Himalaya, India: Geology, v. 34, p. 601–604, doi:10.1130/G22698.1.
Boos, W. R., and Kuang, Z., 2010, Dominant control of south Asian Monsoon by orographic insulation versus plateau heating: Nature, v. 463, p. 218–223, doi:10.1038/nature08707.
Breecker, D. O., Sharp, Z. D., and McFadden, L. D., 2009, Seasonal bias in the formation and stable isotopic compostion of pedogenic carbonate in modern soils from central New Mexico, USA: Geological Society of America Bulletin, v. 121, n. 3/4, p. 630–640, doi:10.1130/B26413.1.
Cerling, T. E., and Quade, J., 1993, Stable carbon and oxygen isotopes in soil carbonates, *in* Swart, P., McKenzie, J. A., and Lohman, K. C., editors, Climate Change in Continental Isotopic Records: Proceedings of Chapman Conference, Jackson Hole, Wyoming: American Geophysical Union Monograph, v. 78, p. 217–231.
Currie, B. S., Rowley, D. B., and Tabor, N. J., 2005, Middle Miocene paleoaltimetry of southern Tibet: Implications for the role of mantle thickening and delamination in the Himalayan orogeny: Geology, v. 33, n. 3, p. 181–184, doi:10.1130/G21170.1.
Cyr, A. J., Currie, B. S., and Rowley, D. B., 2005, Geochemical evaluation of Fenghuoshan Group Lacustrine carbonates, north-central Tibet: Implications for paleoaltimetry of the Eocene Tibetan Plateau: Journal of Geology, v. 113, p. 517–533, doi:10.1086/431907.
DeCelles, P. G., Quade, J, Kapp, P., Fan, M., Dettman, D. L., and Ding, L., 2007, High and dry in central Tibet during the late Oligocene: Earth and Planetary Science Letters, v. 253, p. 389–401, doi:10.1016/j.epsl.2006.11.001.
Dettman, D. L., Fang, X., Garzione, C. N., and Li, J., 2003, Uplift-driven climate change at 12 Ma: a long δ^{18}O record from the NE margin of the Tibetan Plateau: Earth and Planetary Science Letters, v. 214, p. 267–277, doi:10.1016/S0012-821X(03)00383-2.
Garzione, C. N., Quade, J., DeCelles, P. G., and English, N. B., 2000a, Predicting paleoelevation of Tibet and the Himalaya from δ^{18}O vs. altitude gradients in meteoric water across the Nepal Himalaya: Earth and Planetary Science Letters, v. 183, p. 215–229, doi:10.1016/S0012-821X(00)00252-1.
Garzione, C. N., Dettman, D. L., Quade, J., DeCelles, P. G., and Butler, R. F., 2000b, High times on the Tibetan Plateau: Paleoelevation of the Thakkola graben, Nepal: Geology, v. 28, p. 339–342, doi:10.1130/0091-7613(2000)28⟨339:HTOTTP⟩2.0.CO;2.
Garzione, C. N., Dettman, D. L., and Horton, B. K., 2004, Carbonate oxygen isotope paleoaltimetry: evaluating the effect of diagenesis on paleoelevation estimates for the Tibetan Plateau: Palaeogeography, Palaeoclimatology, Palaeoecology, v. 212, p. 119–140, doi:10.1016/j.palaeo.2004.05.020.
Gasse, F., Fontes, J. Ch., Van Campo, E., and Wei, K., 1996, Holocene environmental changes in Bangong Co basin, (Western Tibet). Part 4: Discussion and conclusions: Palaeogeography, Palaeoclimatology, Palaeoecology, v. 120, p. 79–82, doi:10.1016/0031-0182(95)00035-6.
Ghosh, P., Adkins, J., Affek, H., Balta, B., Guo, W., Schauble, E. A., Schrag, D., and Eiler, J. M., 2006a, ^{13}C-^{18}O bonds in carbonate minerals: A new kind of paleothermometer: Geochimica et Cosmochimica Acta, v. 70, p. 1439–1456, doi:10.1016/j.gca.2005.11.014.
Ghosh P., Garzione, C. N., and Eiler, J. M., 2006b, Rapid uplift of the Altiplano revealed in abundances of ^{13}C—^{18}O bonds in paleosol carbonate: Science, v. 311, p. 511–515, doi:10.1126/science.1119365.
Gile, L. H., Peterson, F. F., and Grossman, R. B., 1966, Morphological and genetic sequences of carbonate accumulation in desert soils: Soil Science, v. 101, p. 347–360, doi:10.1097/00010694-196605000-00001.
Graham, S. A., Chamberlain, C. P., Yue, Y., Ritts, B. D., Hanson, A. D., Horton, T. W., Waldbauer, J. R., Poage,

M. A., and Feng, X., 2005, Stable isotope records of Cenozoic climate and topography, Tibetan Plateau and Tarim Basin: American Journal of Science, v. 305, p. 101–118, doi:10.2475/ajs.305.2.101.

Hoke, G. D., Garzione, C. N., Araneo, D. C., Latorre, C., Strecker, M. R., and Williams, K. J., 2009, The stable isotope altimeter: Do Quaternary pedogenic carbonates predict modern elevations?: Geology, v. 37, n. 11, p. 1015–1018, doi:10.1130/G30308A.1.

Hren, M. T., Bookhagen, B., Blisniuk, P. M., Booth, A. L., and Chamberlain, C. P., 2009, $\delta^{18}O$ and δD of streamwaters across the Himalaya and Tibetan Plateau: Implications for moisture sources and paleoelevation reconstructions: Earth and Planetary Science Letters, v. 288, p. 20–32, doi:10.1016/j.epsl.2009.08.041.

Huntington, K. W., Eiler, J. M., Affek, H. P., Guo, W., Bonifacie, M., Yueng, L. Y., Thiagarajan, N., Passey, B., Tripati, A., Daëron, M., and Came, R., 2009, Methods and limitations of "clumped" CO_2 isotope (Δ_{47}) analysis by gas-source isotope ratio mass spectrometry: Journal of Mass Spectrometry, v. 44, n. 9, p. 1318–1329, doi:10.1002/jms.1614.

Hurtado, Jr., J. M., Hodges, K. V., and Whipple, K. X., 2001, Neotectonics of the Thakkhola graben and implications for recent activity on the South Tibetan fault system in the central Nepal Himalaya: Geological Society of America Bulletin, v. 113, p. 222–240, doi:10.1130/0016-7606(2001)113⟨0222: NOTTGA⟩2.0.CO;2.

Kapp, P., Yin, A., Harrison, T. M., and Ding, L., 2005, Cretaceous-Tertiary shortening, basin development, and volcanism in central Tibet: Geological Society of America Bulletin, v. 117, n. 7/8, p. 865–878, doi:10.1130/B25595.1.

Kapp, P., DeCelles, P. G., Leier, A. L., Fabijanc, J. M., He, S., Pullen, A., and Gehrels, G. E., 2007, The Gangdese retroarc thrust belt revealed: GSA Today, v. 17, n. 7, p. 4–9, doi:10.1130/GSAT01707A.1.

Kent-Corson, M. L., Ritts, B. D., Zuang, G., Bovet, P. M., Graham, S. A., and Chamberlain, C. P., 2009, Stable isotopic constraints on the tectonic, topographic, and climatic evolution of the northern margin of the Tibetan Plateau: Earth and Planetary Science Letters, v. 282, p. 158–166, doi:10.1016/j.epsl.2009.03.011.

Kim, S.-T., and O'Neil, J. R., 1997, Equilibrium and non-equilibrium oxygen isotope effects in synthetic carbonates: Geochimica et Cosmochimica Acta, v. 61, p. 3461–3475, doi:10.1016/S0016-7037(97)00169-5.

Lear, C. H., Elderfield, H., and Wilson, P. A., 2000, Cenozoic deep-sea temperatures and global ice volumes from Mg/Ca in benthic foraminiferal calcite: Science, v. 287, p. 269–272, doi:10.1126/science.287.5451.269.

Leier, A., Quade, J., DeCelles, P., and Kapp, P., 2009, Stable isotopic results from paleosol carbonate in south Asia: paleoenvironmental reconstructions and selective alteration: Earth and Planetary Science Letters, v. 279, p. 242–254, doi:10.1016/j.epsl.2008.12.044.

Molnar, P., and Stock, J. M., 2009, Slowing of India's convergence with Eurasia since 20 Ma and its implications for Tibetan mantle dynamics: Tectonics, v. 28, TC 3001, doi:10.1029/2008TC002271.

Mügler, I., Gleixner, G., Günther, F., Mäusbacher, R., Daut, G., Schütt, B., Berking, J., Schwalb, A., Schwark, L., Xu, B., Yao, T., Zhu, L., and Yi, C., 2010, A multi-proxy approach to reconstruct hydrological changes and Holcene climate development of Nam Co, Central Tibet: Journal of Paleolimnology, v. 43, p. 625–648, doi:10.1007/s10933-009-9357-0.

Murphy, M. A., Yin, A., Harrison, T. M., Dürr, S. B., Chen, Z., Ryerson, F. J., Kidd, W. S. F., Wang, X., and Zou, X., 1997, Did the Indo-Asian collision alone create the Tibetan Plateau?: Geology, v. 25, n. 8, p. 719–722, doi:10.1130/0091-7613(1997)025⟨0719:DTIACA⟩2.3.CO;2.

Passey, B. H., Levin, N. E., Cerling, T. E., Brown, F. H., and Eiler, J. M., 2010, High-termperature environments of human evolution in East Africa based on bond ordering in paleosol carbonates: Proceedings of the National Academy of Sciences of the United States of America, v. 107, n. 25, p. 11245–11249, doi:10.1073/pnas.1001824107.

Poage, M. A., and Chamberlain, C. P., 2001, Empirical relationships between elevation and the stable isotope composition of precipitation and surface waters: Considerations for studies of paleoelevation change: American Journal of Science, v. 301, p. 1–15, doi:10.2475/ajs.301.1.1.

Polissar, P. J., Freeman, K. H., Rowley, D. B., McInerney, F. A., and Currie, B. S., 2009, Paleoaltimetry of the Tibetan Plateau from D/H ratios of lipid biomarkers: Earth and Planetary Science Letters, v. 287, p. 64–76, doi:10.1016/j.epsl.2009.07.037.

Quade, J., Cerling, T. E., and Bowman, J. R., 1989a, Systematic variation ins the carbon and oxygen isotopic composition of pedogenic carbonate along elevation transects in the southern Great Basin, United States: Geological Society of America Bulletin, v. 101, p. 464–475, doi:10.1130/0016-7606(1989)101⟨0464: SVITCA⟩2.3.CO;2.

——— 1989b, Development of the Asian Monsoon revealed by marked ecological shift during the latest Miocene in northern Pakistan: Nature, v. 342, p. 163–166, doi:10.1038/342163a0.

Quade, J., Garzione, C., and Eiler, J., 2007, Paleoelevation reconstruction using Pedogenic Carbonates, *in* Kohn, M., editor, Paleoaltimetry: Geochemical and Thermodynamic approaches: Reviews in Mineralogy and Geochemistry, v. 66, p. 53–87, doi:10.2138/rmg.2007.66.3.

Rowley, D. B., and Currie, B. S., 2006, Palaeo-altimetry of the late Eocene to Miocene Lunpola basin, central Tibet: Nature, v. 439, p. 677–681, doi:10.1038/nature04506.

Rowley, D. B., and Garzione, C. N., 2007, Stable isotope-based paleoaltimetry: Annual Review of Earth and Planetary Sciences, v. 35, p. 463–508, doi:10.1146/annurev.earth.35.031306.140155.

Rowley, D. B., Pierrehumbert, R. T., and Currie, B. S., 2001, A new approach to stable isotope-based paleoaltimetry: implications for paleoaltimetry and paleohypsometry of the High Himalaya since the Late Miocene: Earth and Planetary Science Letters, v. 188, p. 253–268, doi:10.1016/S0012-821X(01)00324-7.

Rozanski, K, Araguás-Araguás, L., and Gonfiantini, R., 1993, Isotopic Patterns in Modern Global Precipitation, *in* Swart, P., McKenzie, J. A., and Lohman, K. C., editors, Climate Change in Continental Isotopic

Records: Proceedings of Chapman Conference, Jackson Hole, Wyoming, American Geophysical Union Monograph, v. 78, p. 1–36.

Saylor, J. E., Quade, J., Dettman, D. L., DeCelles, P. G., Kapp, P. A., and Ding, L., 2009, The Late Miocene through present paleoelevation history of southwestern Tibet: American Journal of Science, v. 309, p. 1–42, doi:10.2475/01.2009.01.

Thompson, L. G., Mosley-Thompson, E., Davis, M. E., Lin, P.-N., Henderson, K., and Mashiotta, T. A., 2003, Tropical glacier and ice core evidence of climate change on annual to millennial time scales: Climatic Change, v. 59, p. 137–155, doi:10.1023/A:1024472313775.

Tian, L., Masson-Delmotte, V., Stievenard, M., Yao, T., and Jouzel, J., 2001, Tibetan Plateau summer monsoon northward extent revealed by measurements of water stable isotopes: Journal of Geophysical Research, v. 106, p. 28,081–28,088, doi:10.1029/2001JD900186.

Tian, L., Yao, T., White, J. W. C., Yu, W., and Wang, N., 2005, Westerly moisture transport to the middle of Himalayas revealed from the high deuterium excess: Chinese Science Bulletin, v. 50, p. 1026–130, doi:10.1360/04wd0030.

Tian, L., Yao, T., MacClune, K., White, J. W. C., Schilla, A., Vaughn, B., Vachon, R., and Ichiyanagi, 2007, Stable isotopic variations in west China: A consideration of moisture sources: Journal of Geophysical Research: v. 112, D10112, doi:10/1029/2006JD007718.

Volkmer, J. E., Kapp, P., Guynn, J. H., and Lai, Q., 2007, Cretaceous-Tertiary structural evolution of the north-central Lhasa Terrane, Tibet: Tectonics, TC6007, doi:10.1029/2005TC001832.

Wang, Y., Deng, T., and Blasatti, D., 2006, Ancient diets indicate significant uplift of southern Tibet after ca. 7 Ma: Geology, v. 34, p. 309–312, doi:10.1130/G22254.1.

Zachos, J. C., Stott, L. D., and Lohmann, K. C., 1994, Evolution of early Cenozoic marine temperatures: Paleoocenaography, v. 9, n. 2, p. 353–387, doi:10.1029/93PA03266.

Zhang, X., Nakawo, M., Yao, T., Han, J., and Xie, Z., 2002, Variations of stable isotopic compositions in precipitation on the Tibetan Plateau and its adjacent regions: Science in China (Series D), v. 45, n. 6, p. 481–493, doi:10.1360/02yd9050.